



Article

# Microbial Consortia and Mixed Plastic Waste: Pangenomic Analysis Reveals Potential for Degradation of Multiple Plastic Types via Previously Identified PET Degrading Bacteria

Sabrina Edwards <sup>1</sup>, Rosa León-Zayas <sup>2</sup>, Riyaz Ditter <sup>1</sup>, Helen Laster <sup>1</sup>, Grace Sheehan <sup>2</sup>, Oliver Anderson <sup>2</sup>, Toby Beattie <sup>1</sup> and Jay L. Mellies <sup>1,\*</sup>

<sup>1</sup> Biology Department, Reed College, Portland, OR 97202, USA; sabrinaredwards@reed.edu (S.E.); ditter@reed.edu (R.D.); lasterh@reed.edu (H.L.); tobeattie@reed.edu (T.B.)

<sup>2</sup> Biology Department, Willamette University, Salem, OR 97301, USA; rleonazayas@willamette.edu (R.L.-Z.); gasheehan@willamette.edu (G.S.); ofanderson@willamette.edu (O.A.)

\* Correspondence: jay.mellies@reed.edu; Tel.: +1-503-517-7964

**Abstract:** The global utilization of single-use, non-biodegradable plastics, such as bottles made of polyethylene terephthalate (PET), has contributed to catastrophic levels of plastic pollution. Fortunately, microbial communities are adapting to assimilate plastic waste. Previously, our work showed a full consortium of five bacteria capable of synergistically degrading PET. Using omics approaches, we identified the key genes implicated in PET degradation within the consortium's pangenome and transcriptome. This analysis led to the discovery of a novel PETase, EstB, which has been observed to hydrolyze the oligomer BHET and the polymer PET. Besides the genes implicated in PET degradation, many other biodegradation genes were discovered. Over 200 plastic and plasticizer degradation-related genes were discovered through the Plastic Microbial Biodegradation Database (PMBD). Diverse carbon source utilization was observed by a microbial community-based assay, which, paired with an abundant number of plastic- and plasticizer-degrading enzymes, indicates a promising possibility for mixed plastic degradation. Using RNAseq differential analysis, several genes were predicted to be involved in PET degradation, including aldehyde dehydrogenases and several classes of hydrolases. Active transcription of PET monomer metabolism was also observed, including the generation of polyhydroxyalkanoate (PHA)/polyhydroxybutyrate (PHB) biopolymers. These results present an exciting opportunity for the bio-recycling of mixed plastic waste with upcycling potential.

**Keywords:** biodegradation; poly(ethylene)terephthalate (PET); polyhydroxyalkanoate (PHA); plasticizers; mixed plastics; pangenomes



**Citation:** Edwards, S.; León-Zayas, R.; Ditter, R.; Laster, H.; Sheehan, G.; Anderson, O.; Beattie, T.; Mellies, J.L. Microbial Consortia and Mixed Plastic Waste: Pangenomic Analysis Reveals Potential for Degradation of Multiple Plastic Types via Previously Identified PET Degrading Bacteria. *Int. J. Mol. Sci.* **2022**, *23*, 5612. <https://doi.org/10.3390/ijms23105612>

Academic Editor: Irina Moreira

Received: 28 April 2022

Accepted: 13 May 2022

Published: 17 May 2022

**Publisher's Note:** MDPI stays neutral with regard to jurisdictional claims in published maps and institutional affiliations.



**Copyright:** © 2022 by the authors. Licensee MDPI, Basel, Switzerland. This article is an open access article distributed under the terms and conditions of the Creative Commons Attribution (CC BY) license (<https://creativecommons.org/licenses/by/4.0/>).

## 1. Introduction

Currently, it is estimated that nearly 80% of all plastic ever made will be discarded into landfills or as pollution within our ecosystems, and this percentage is rapidly increasing [1]. Globally, over 380 million metric tons of plastic are produced each year, and 10 million metric tons end up in our oceans annually [2]. Fifty percent of this material is made for single-use purposes, and the COVID-19 pandemic ultimately created an even greater demand for single-use plastics, which only exacerbated the plastic pollution crisis [3,4]. Continuing at this pace, it is estimated that by 2050, by weight, there will be more plastics in our oceans than fish [5]. The widespread pollution caused by plastics and microplastics is ubiquitous [1]. They have been found within humans [6] and many other organisms [7], in virtually all the environmental locations that have been tested [8–10], and even dispersed in rainwater [11].

Polyethylene terephthalate (PET), polyurethane (PUR), polyethylene (PE), polyamide (PA), polystyrene (PS), polyvinylchloride (PVC), and polypropylene (PP) comprise the

majority of manufactured plastics [12]. Fortunately, within the microbial world, enzymes exist to degrade naturally occurring compounds, such as lignin, that are chemically similar to synthetic polymers [13,14], and the microbes encoding these enzymes are found in both marine and terrestrial environments [15]. Of these polymers, there has been a concerted effort to identify PETases to degrade recycled water bottles and other single-use containers, improve their activity through the modification of active sites, and improve thermal stability. In 2016, from a plastics recycling facility in Japan, Yoshida et al. isolated *Ideonella sakaiensis* that encoded a PETase and a second enzyme, MHETase, involved in the stepwise degradation of PET [16]. *I. sakaiensis* was determined to exist as part of a consortium of microbes and was able to use PET as a sole source of carbon and energy [17]. Taking a metagenomics approach, researchers who were studying leaf compost identified a cutinase (LCC) that was also able to degrade PET [18].

Further research shows the benefits of using microbial consortia for bioremediation due to their mixed metabolism within native bacterial communities [19]. Consortia of environmental microbiomes have been documented to enzymatically and synergistically degrade petroleum and petroleum-derived products such as plastics [20–26]. Previously, we isolated a microbial consortium from petroleum-contaminated soils comprised of five *Pseudomonas* and *Bacillus* spp. that showed the synergistic degradation of PET [25]. Sequencing revealed that these strains had unique and diverse genomes with many enzymes with hydrolytic activities [27]. However, the genetics behind the mixed metabolism and observed synergy amongst these strains had not been fully realized. By employing pangenomic analysis, our goal was to identify the core gene clusters responsible for PET degradation, as well as other plastic-degrading genes and pathways from our previously described consortia of bacteria [25].

A pangenome is the collective set of genes shared by all strains of a species [28]. It contains a core genome with all the genes shared by the same species, such as essential metabolic genes and regulatory functions, and a variable genome. The variable genome within a pangenome are those genes that are present in two or more strains; they are often genes from specific adaptations within their environment and are not found within the core genome [29,30]. By using reference genomes of closely related species that were not identified to degrade PET, the gene clusters shared amongst the consortia members were analyzed to give insight into their adaptive evolution toward plastic degradation [31,32].

Additionally, studying transcriptomics of consortia can be a powerful tool to identify the active RNA transcripts under restrictive conditions, such as growth on a single carbon source like PET [33–35]. Our results identify the genetic pathways within the *Pseudomonas* and *Bacillus* spp. that, in part, explain the synergistic degradation of PET. These data regarding bacteria residing in petroleum-polluted soils revealed a wealth of enzymes that are predicted [36] to be associated with the biodegradation of multiple types of biological and synthetic plastic polymers.

## 2. Results

### 2.1. Employing Pangenomic Analysis toward Understanding Synergistic PET Degradation

Previously, our group provided experimental evidence that a full consortium of three *Pseudomonas* and two *Bacillus* spp. collected from hydrocarbon-polluted soil could synergistically degrade polyethylene terephthalate (PET) [25]. Due to this observed synergy, we sought to examine the pangenome encoded by the full consortium to gain deeper insight into how they might be degrading PET genetically and metabolically.

In this analysis, the 232 core genomes (i.e., all *Pseudomonas* (144) and *Bacillus* (88) species within the MicroScope platform database [37] (excluding the five strains within our full consortium) at the time of this analysis) were purposefully excluded (Supplemental Figure S1). The parameters were set using 50% amino acid (aa) identity and 80% alignment coverage. After the exclusion of the core genome found in all *Pseudomonas* and *Bacillus* spp. within the database, 259 gene groups were found to be shared in the core genome within the pangenome of these five strains (Figure 1).

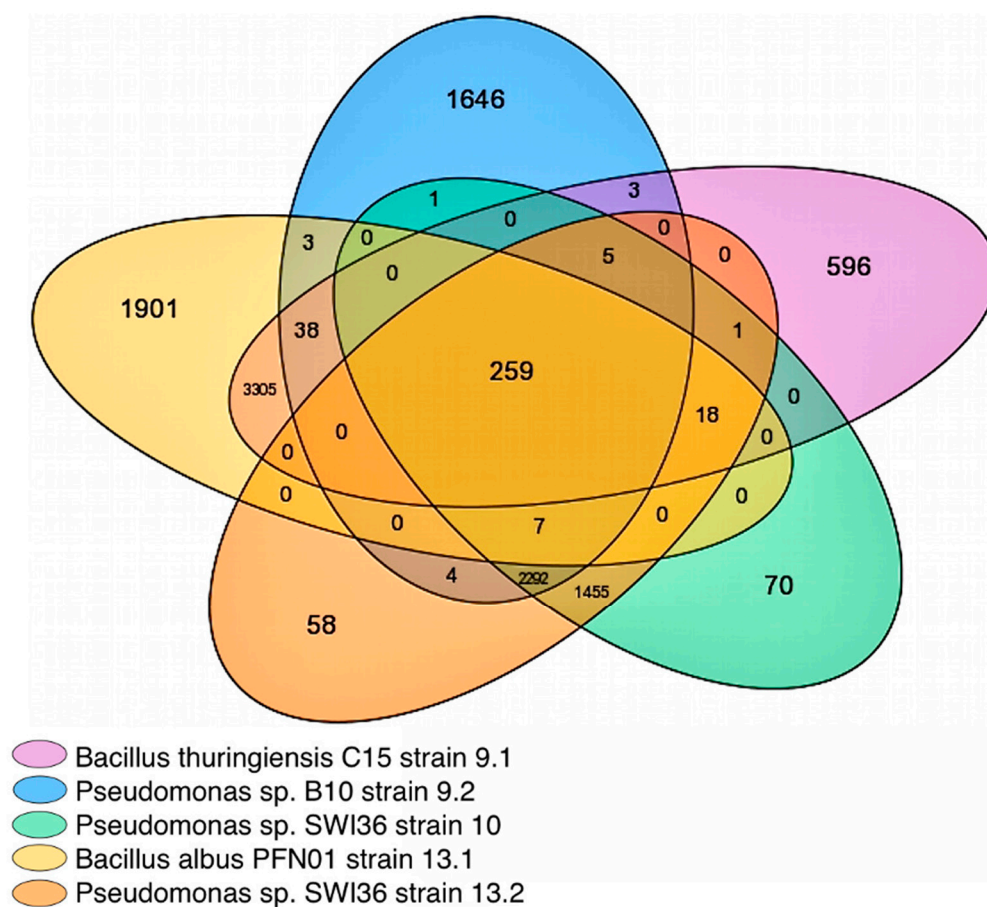


**Figure 1.** Venn diagram illustrating the number of genes within the pangenome of all five bacterial strains. Pangenome gene clusters were analyzed using MicroScope gene families (MICFAM), computed with the SiLiX softwares [38]. Genes were considered orthologs if genes contained >50% amino acid sequence similarity and 80% alignment coverage. Diagram generated by MicroScope platform with Creative Commons Attribution 4.0 International License, public use.

*Bacillus albus* PFN01 strain 13.1 and *Pseudomonas* sp. B10 strain 9.2 had the most diverse set of accessory genes (Supplemental File S1) compared to all other strains within the full consortium indicating clear differences between the consortia members. *Bacillus* strains 9.1 and 13.1 share a large pangenome of over 3305 genes. The pangenome of all three *Pseudomonas* strains contained over 2292 shared genes. When comparing *Pseudomonas* strain 10 and 13.2, it was established that strain 10 contained 70 unique, species-specific hypothetical proteins different from the pangenome, while 13.2 contained 58 different genes, despite species relation.

Initially, within the core pangenome, several gene groups were of interest, including aldehyde dehydrogenases, esterases, and alcohol dehydrogenases (Supplemental Figure S2). Prior to RNA sequencing and database analysis, these genes were predicted to be involved in PET degradation, as dehydrogenases and esterases have been implicated in PET oligomer and monomer degradation, but the specific enzymes responsible had yet to be confirmed.

## 2.2. Esterase *EstB* in Strain 9.2 Is Active against PET

An esterase encoded in the *estB* gene identified within the pangenome was discovered and explored. Previously, researchers discovered that an *estB* encoded in *Enterobacter* sp. HY1 could degrade BHET [39]. With this in mind, a deletion mutant of esterase gene *estB* ( $\Delta estB$ ) in strain *Pseudomonas* 9.2 was created using *pEX18Tc sacB* suicide plasmid to test if it could cleave BHET [40]. This  $\Delta estB$  mutant showed significantly decreased esterase

activity on 4-nitrophenyl butyrate (p-np-butyrate) (Figure 2a). To confirm p-np-butyrate activity, the purified EstB protein resulted in increased p-np-butyrate cleavage, illustrated in Figure 2b.

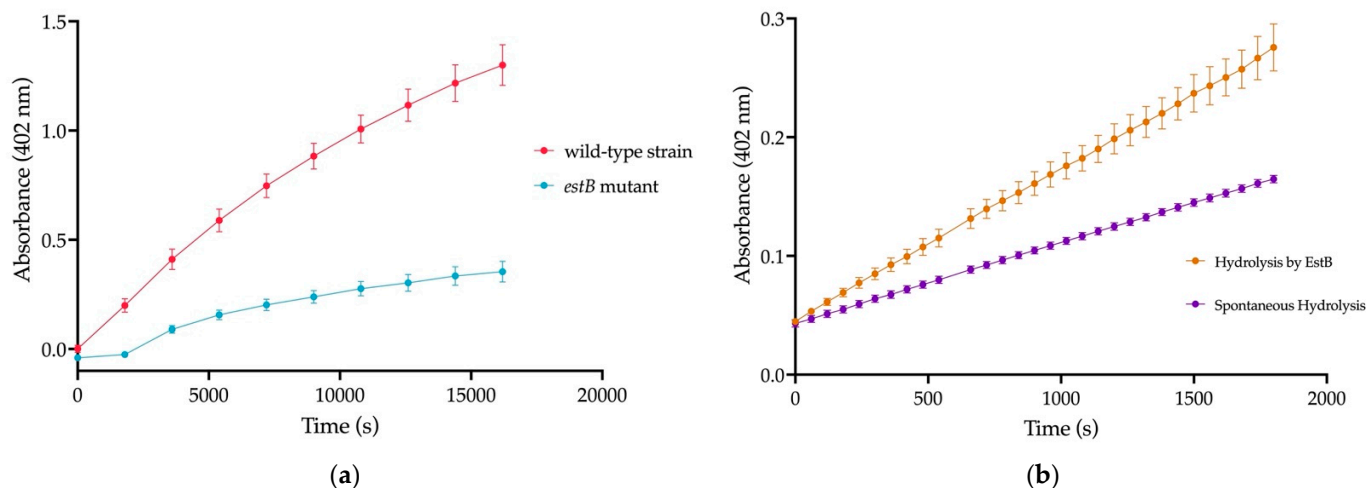


**Figure 2.** 4-Nitrophenyl Butyrate (p-np butyrate) Assay to determine esterase activity (a) Deletion of *estB* resulted in significant decrease in activity against np-butyrate indicating loss of esterase activity; (b) Purified EstB resulted in significant hydrolysis of np-butyrate, indicating this protein possesses esterase activity.

The purified EstB was then incubated on either BHET (Figure 3a) or micro-PET (Figure 3b). The hydrolysis byproducts from both compounds were confirmed via HPLC, with the increased absorbance at 245 nm indicating the presence of oligomer MHET and monomer TPA.

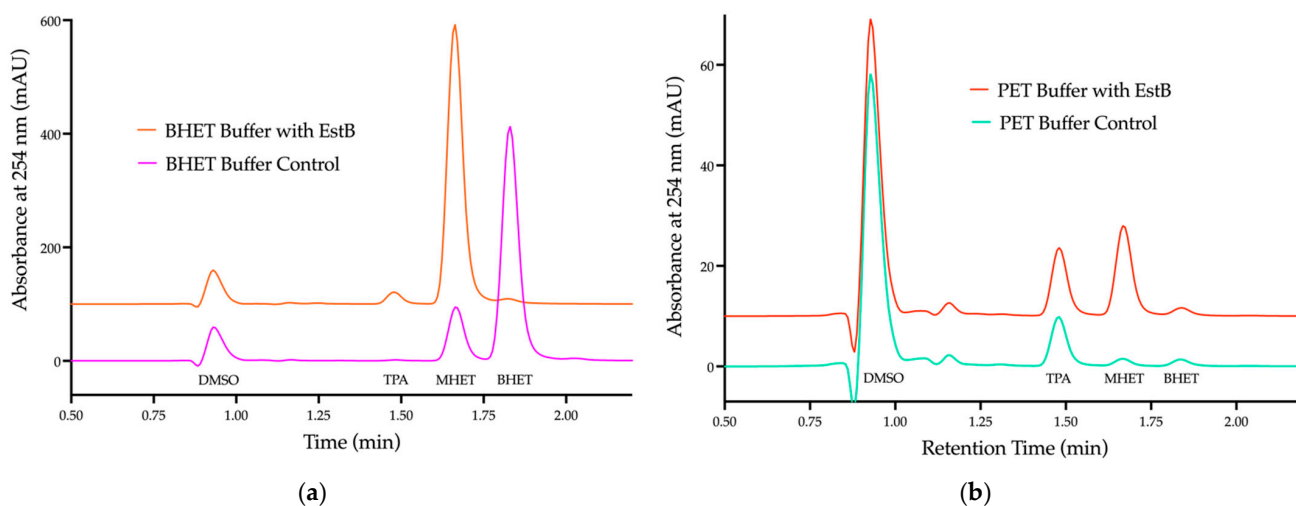


**Figure 3.** HPLC chromatogram of hydrolysis byproducts from purified EstB incubated on BHET and micro-PET (a) Protein EstB incubated on BHET showing significant MHET and TPA accumulation ( $p < 0.0001$ ) (b) Protein EstB incubated on PET showing significant MHET accumulation ( $p < 0.0001$ ). All samples were conducted in triplicate and averaged, there was no significant difference between replicates.

The incubation of EstB on BHET results in a statistically significant decrease in BHET peak area ( $p < 0.0001$ ), coupled with a statistically significant increase in the MHET peak area ( $p < 0.0001$ ) (Figure 3b). There was also a statistically significant increase in the TPA

peak area ( $p < 0.0001$ ), although this is likely a result of the spontaneous hydrolysis of MHET. This is because EstB largely shows no activity against MHET, and the hydrolytic cleavage of BHET would only yield MHET and EG, not TPA. All three monomers are present in the micro-PET solution prior to the addition of EstB, which is likely a result of hydrolysis from the micro-PET production procedure in which TFA was used to dissolve the PET plastic.

The addition of EstB to the micro-PET solution results in a statistically significant increase in both the MHET and the TPA peak areas ( $p < 0.0001$ ), but no change in the BHET peak area. The absence of an increase in the BHET peak area indicates that any BHET freed from PET cleavage is subsequently hydrolyzed to MHET. TPA is expected to be released from the hydrolysis of PET due to different oligomer and monomer products being released, depending on which ester bonds are cleaved (Supplemental Figure S2). While EG is not detected via HPLC spectra at 254 nm, it is assumed to be in the solution, as the cleavage of BHET to MHET releases EG.

In order to conduct preliminary structure analyses of EstB, its 3D structure was predicted with a computational AI system called AlphaFold v2.0 [41]. AlphaFold predicts the 3D structure of a protein from just its amino acid sequence by incorporating novel neural network architectures and training procedures based on homology to solve structural, evolutionary, physical, and geometric constraints [41]. The structure of EstB belongs to the  $\alpha/\beta$  hydrolase superfamily and contains the conserved serine hydrolase Gly-X-Ser-X-Gly (Gly112- Phe113-Ser114-Gln115-Gly116) located at the active site [42], with the residues Asp168 and His199 completing the catalytic triad.

As EstB shares the same activity on PET and BHET as the PETase of *Ideonella sakaiensis* [43], degrading PET and BHET to form MHET, the two enzymes were subsequently compared on a structural level. The *IsPETase* has an L-shaped hydrophobic binding cleft that binds the PET polymer, with hydrolytic cleavage occurring at the catalytic serine residue. The dimensions of this cleft are roughly 40 Å in length and 29 Å in width. A similar hydrophobic cleft was identified in EstB, extending from the catalytic triad. The dimensions of this cleft are approximately 33 Å in length and 30 Å in width (Figure 4). Based on the mutational analysis, the assays using a purified protein, and the initial structural analysis, we concluded that EstB of *Pseudomonas* strain 9.2 is indeed a PETase.

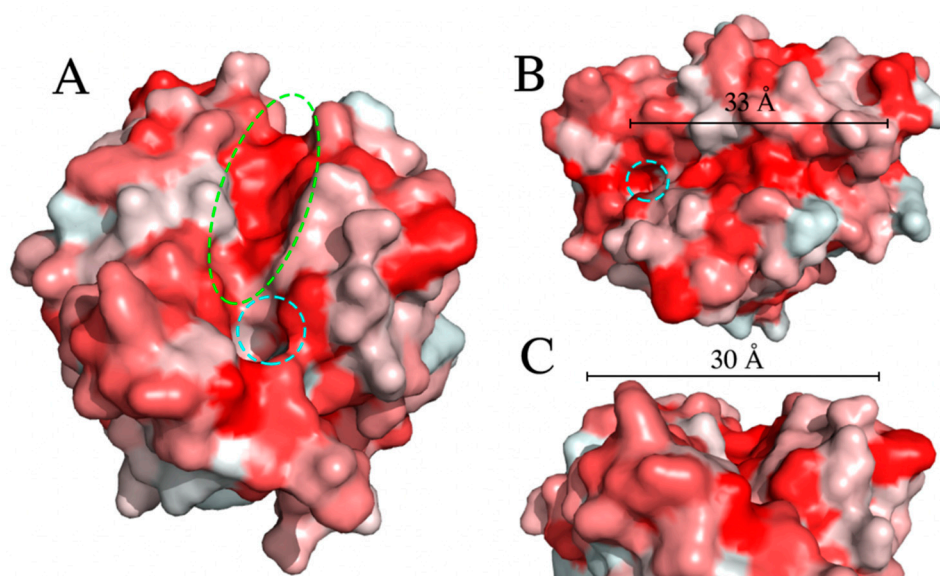


**Figure 4.** Hydrophobicity surface model of EstB. Red indicates hydrophobic regions; white indicates hydrophilic regions. (A) Front view of the potential substrate binding site of EstB. Catalytic residue Ser114 is indicated by dotted cyan circle, binding cleft is indicated dotted green circle. (B) Length of binding cleft. Catalytic residue S114 is indicated by dotted cyan circle. (C) Width of binding cleft.

### 2.3. Identification of Predicted Plastic Degrading Genes Using PMBD

The annotated amino acid FASTA file generated above from pangenomic analysis was used to mine for genes with plastic-degrading potential using the Plastic Metabolic Biodegradation Database (PMBD) [36]. Within the pangenome, 250 genes were predicted to be involved with plastic degradation (Supplemental File S2). These genes consisted mostly of hydrolases and oxidoreductases of various enzyme classes (Supplemental File S3), but also included regulatory proteins, essential transferases, lyases, and isomerases/translocases crucial to downstream monomer assimilation.

### 2.4. Genes Implicated in PET Degradation

The oligomers BHET/MHET and the polymer PET have been previously identified to be hydrolyzed via esterase/hydrolase activity. Two predicted PET hydrolases encoded in *Streptomyces* sp. shared more than 23% identity to alpha/beta hydrolases/dienelactone hydrolase encoded in *Bacillus* strain 9.1 and in *Pseudomonas* strains 10/13.2. Additionally, three enzymes within four of the five strains, the exception being strain *Bacillus* 13.1, were predicted to have feruloyl esterase activity; these enzymes were annotated as cellulose-binding proteins, with two being feruloyl esterases, according to UniProt (Table 1). The esterase EstB was one of three enzymes identified as having feruloyl esterase activity.

**Table 1.** Predicted plastic biodegradation enzymes with significant percentage identity and similarity to genes encoded within the pangenome of the full consortium.

Plastic	Enzyme	Species	Uniprot ID	% Identity	E-Value	Bit-Score	Strain
PET	Aldehyde dehydrogenase	<i>Mycobacterium vanbaalenii</i>	Q9KHU2	33.97	$8.23 \times 10^{-74}$	239	all
	Cellulose-binding protein	<i>Micromonospora rifamycinica</i>	A0A120F7D2	27.98	$8.59 \times 10^{-4}$	37.7	10/13.2
	Feruloyl Esterase	<i>Phialocephala subalpina</i>	A0A1L7XXB0	32.00	$1.43 \times 10^{-4}$	39.7	9.2
	Feruloyl Esterase	<i>Rhynchosporium secalis</i>	A0A1E1MSN7	27.89	$5.65 \times 10^{-5}$	42.7	9.1
	Poly(ethylene terephthalate) hydrolase	<i>Streptomyces</i> sp. 111WW2	A0A2P8AA05	23.77	$2.93 \times 10^{-5}$	43.1	10/13.2
	Poly(ethylene terephthalate) hydrolase	<i>Streptomyces</i> sp. MH60	A0A2S6X119	23.75	$7.52 \times 10^{-6}$	45.4	9.1
	Putative terephthalate 1,2-dioxygenase	<i>Rhodococcus</i> sp. DK17	Q6REK1	32.30	$6.62 \times 10^{-33}$	127	9.2/10/13.2
	TPA 1,2-dioxygenase, reductase component 1	<i>Comamonas</i> sp.	TPDR1	34.92	$3.46 \times 10^{-5}$	43.1	9.2/10/13.2
	TPA 1,2-dioxygenase, reductase component 2	<i>Comamonas</i> sp.	TPDR2	36.51	$6.73 \times 10^{-6}$	45.4	9.2/10/13.2
	TPA 1,2-dioxygenase, oxygenase alpha 1	<i>Comamonas</i> sp.	TPDA1	34.10	$2.15 \times 10^{-29}$	117	9.2/10/13.2
	TPA 1,2-dioxygenase oxygenase alpha 2	<i>Comamonas</i> sp.	TPDA2	34.10	$2.21 \times 10^{-29}$	117	9.2/10/13.2
	Twin-arginine translocation pathway signal	<i>Polaromonas</i> sp. strain JS666	Q12BN2	39.46	$5.89 \times 10^{-25}$	103	9.2/10/13.2
	Glyoxalase	<i>Azoarcus</i> sp. PA01	A0A0M0FWC0	26.471	$1.19 \times 10^{-4}$	37.7	9.1/13.1
PLA	PLA depolymerase	uncultured bacterium	A4UZ10	46.71	$1.49 \times 10^{-124}$	365	9.1/13.1
	PLA depolymerase	uncultured bacterium	A4UZ14	37.46	$6.05 \times 10^{-67}$	211	9.2/10/13.2
	PLA depolymerase (Fragment)	uncultured bacterium	A4UZ11	48.5	$1.80 \times 10^{-123}$	362	9.1/9.2/13.1
PUR	Polyurethanase	<i>Pseudomonas</i> sp. FW305-BF6	A0A2N8H9Y3	99.51	0.00	1225	9.2
	Polyurethanase	<i>Pseudomonas fluorescens</i>	A0A0C2A4M0	59.52	$8.28 \times 10^{-7}$	52	10/13.2
	Polyurethanase (Fragment)	<i>Pseudomonas</i> sp. DrBHI1	A0A246GXG4	66.61	0.00	733	9.2/10/13.2
	Polyurethanase A	<i>Pseudomonas</i> sp. Os17	A0A0D6BHI0	77.96	0.00	994	9.2
PVA	Polyvinyl alcohol dehydrogenase	<i>Pseudomonas</i> sp. FW305-BF6	A0A2N8GY02	98.23	0.00	561	9.2
	Polyvinyl alcohol dehydrogenase	<i>Xanthomonas arboricola</i>	A0A2S6Y8G0	37.5	$4.65 \times 10^{-4}$	41.2	10/13.2
	Polyvinyl alcohol dehydrogenase (Fragment)	<i>Opitutae bacterium</i>	A0A2D6VIL8	27.63	$1.89 \times 10^{-4}$	40.8	10/13.2
	Oxidized polyvinyl alcohol hydrolase	<i>Syntrophorhabdus</i> sp. PtaB	A0A1V4WJ12	30.07	$2.92 \times 10^{-10}$	57	9.1/9.2/13.1
	Probable polyvinyl alcohol dehydrogenase	<i>Streptomyces rochei</i>	Q83X81	36.15	$1.60 \times 10^{-6}$	49.3	9.2/10/13.2
	PVA dehydrogenase PQQ dependent	<i>Bradyrhizobium</i> sp.	A0A160UKB5	28.36	$4.92 \times 10^{-4}$	41.6	9.2/10/13.2
PHA PHB	Poly(3-hydroxyalkanoate) depolymerase	<i>Pseudomonas fluorescens</i>	A0A0C1ZS59	100.00	0.00	577	9.2
	Poly(3-hydroxyalkanoate) depolymerase	<i>Pseudomonas putida</i> S12	A0A0A7PVK5	99.65	0.00	574	10.13.2
	Poly(3-hydroxybutyrate) depolymerase	<i>Haladaptatus paucihalophilus</i>	E7QQJ1	50.73	$2.83 \times 10^{-8}$	55.5	9.1
	Poly(3-hydroxybutyrate) depolymerase	<i>Marinobacter lutaensis</i>	A0A1V2DRR5	46.67	$5.28 \times 10^{-24}$	85.1	9.2
	Poly(3-hydroxyalkanoate) depolymerase C	<i>Paenibacillus polymyxa</i>	A0A2X1WPU8	44.53	$4.46 \times 10^{-114}$	338	9.1
	Poly(3-hydroxybutyrate) depolymerase	<i>Marinobacter</i> sp. AC-23	A0A152CI13	44.44	$6.19 \times 10^{-17}$	67.4	10/13.2
	Poly(3-hydroxyalkanoate) depolymerase	<i>Pseudomonas fluorescens</i> strain Pf0-1	Q3KCH8	44.19	$1.09 \times 10^{-4}$	40.8	13.1
	Poly(3-hydroxybutyrate) depolymerase	<i>Bacillus megaterium</i> ATCC12872	D5DZL2	43.26	$2.37 \times 10^{-83}$	251	13.1
	Poly(3-hydroxyalkanoate) synthase	<i>Paracoccus denitrificans</i>	Q9WX80	33.51	$9.86 \times 10^{-98}$	308	all

Monomers of PET, terephthalic acid (TPA), and ethylene glycol (EG) were previously identified as being assimilated by the full consortium [25]. Analysis shows (Table 1) that

the *Pseudomonas* spp. strains encoded dioxygenases/reductase complexes with greater than 34% identity to previously identified TPA dioxygenases in *Comamonas* sp. [33], as well as other dioxygenases complexes (Table 3) that may be responsible for TPA degradation. We predicted that aldehyde dehydrogenases and/or alcohol dehydrogenases encoded within the genomes of the full consortium would be involved in the biodegradation EG. Aldehyde dehydrogenases have been implicated in poly(ethylene) glycol (PEG) and EG metabolism, as well as implicated in the surface modification of PET plastic [35,44,45] Identified from this analysis, an encoded aldehyde dehydrogenase had nearly 34% identity to petroleum-degrading *Mycobacterium vanbaalenii*. As these organisms were collected from oil-contaminated soils, we hypothesized that this or other aldehyde dehydrogenases may be active against petroleum-derived carbon sources, such as PET.

### 2.5. Genes Implicated in the Biodegradation of Other Plastic Types

Despite investigating the pangenome for PET degradation initially, a multitude of identified genes were implicated in the degradation of other plastic types. These types included synthetic PUR and PVA, as well as more biodegradable polymers and biopolymers such as PLA and PHA/PHB (Table 1). Research has shown that several *Pseudomonas* and *Bacillus* species are highly proficient at degrading most polymers and xenobiotics [46–49]. It is possible that several other plastic types might be degradable by our full consortium. Other encoded oxidoreductases and hydrolases (Supplemental File S3) may degrade other plastic types as well, and our group currently has studies underway to determine the full consortium's biodegradation potential.

### 2.6. Genes Implicated in the Biodegradation of Plasticizer and Xenobiotics

We observed a majority of biodegradation enzymes predominately being involved in plasticizer degradation (Table 2). This is in accordance with previous research showing that within the global microbiome, soil microbes, such as these strains, have a higher diversity of plasticizer degradation when compared to marine environments [15]. Several of these oxidoreductases and dehydrogenases were correlated with plasticizers such as polyethylene glycol (PEG) [44] and polypropylene glycol (PPG) [45], as well as xenobiotics such as PAHs and other phenols (Table 2) [50,51].

**Table 2.** Predicted plasticizer and other xenobiotic biodegradation genes with significant percentage identity and similarity to genes encoded in strains within the full consortium.

Enzyme	Species	Uniprot ID	% Identity	E-Value	Bit-Score	Strain
Taurine dioxygenase	<i>Gordonia phthalatica</i>	A0A0N9N9P8	68.09	$3.71 \times 10^{-146}$	410	9.2/10/13.2
2-nitropropanedioxygenase	<i>Gordonia phthalatica</i>	A0A0N9N4Y4	51.10	$1.02 \times 10^{-83}$	254	all
Tert-butyl alcohol monooxygenase reductase	<i>Aquicola tertiaricarbonis</i>	G8FRC6	44.59	$2.50 \times 10^{-84}$	255	all
4,4'-diaponeurosporenoateglycosyltransferase	<i>Bacillus enclensis</i>	A0A0V8HPX8	44.05	$3.17 \times 10^{-10}$	60.5	all
Phenol hydrolase reductase	<i>Methylibium petroleiphilum</i>	A2SI47	41.38	$4.97 \times 10^{-11}$	61.2	all
2-hydroxy-6-oxo-6-(2'-carboxyphenyl)-hexa-2,4-dienoate hydrolase	<i>Terrabacter</i> sp. strain DBF63	Q83ZF0	38.46	$1.06 \times 10^{-18}$	82.4	all
Tert-butyl alcohol monooxygenase	<i>Aquicola tertiaricarbonis</i>	G8FRC5	38.18	$1.27 \times 10^{-4}$	37.7	9.2/10/13.1/13.2
Quercetin 2,3-dioxygenase	<i>Gordonia phthalatica</i>	A0A0N9MT24	37.16	$2.99 \times 10^{-34}$	121	all
NidB2	<i>Mycobacterium vanbaalenii</i>	Q6H2J5	37.04	$2.1 \times 10^{-10}$	54.3	9.2/10/13.2
Naphthalene inducible dioxygenase	<i>Mycobacterium vanbaalenii</i>	Q9KHU1	35.64	$3.51 \times 10^{-43}$	155	9.2/10/13.1/13.2
5,5'-dehydrodivanillateO-demethylase	<i>Paraburkholderia tropica</i>	A0A1A5XFM6	34.38	$4.84 \times 10^{-18}$	82	all
Probable phenol hydrolase	<i>Rhodococcus</i> sp. EsD8	N1M644	33.33	$7.2 \times 10^{-8}$	51.6	all
Putative nitropropane dioxygenase	<i>Rhodococcus</i> sp. DK17	Q6REN2	32.84	$2.46 \times 10^{-34}$	127	all
1-hydroxy-2-naphthoicacid dioxygenase	<i>Mycobacterium</i> sp. CH1	C0KUL5	32.65	$7.45 \times 10^{-58}$	190	9.1
Phenol hydrolase	<i>Rhodococcus opacus</i> M213	K8XRS6	29.667	$3.2 \times 10^{-17}$	79	all
2-3DHBA3,4-dioxygenase	<i>Pseudomonas stutzeri</i>	A0A2Z5UC95	29.524	$3.65 \times 10^{-5}$	42.4	10/13.2
Phenanthrene-4,5-dicarboxylate 5-decarboxylase	<i>Pseudonocardia</i> sp. Ae707	A0A1Q8KNT8	27.727	$2.02 \times 10^{-9}$	54.3	9.1/9.2/10/13.2

Phthalate- and paraben-degrading oxidoreductases comprised the majority of plastic-related genes (Table 3). The enzyme class numbers of the specific oxidoreductases and other enzyme types are included in Supplementary Figure S3. Many genes were predicted

to be involved in the degradation of both phenolic acids/phthalates [52] such as TPA [33] and parabens such as 4-hydroxybenzoic acid [53].

**Table 3.** Predicted phthalate plasticizer biodegradation genes with significant percentage identity and similarity to genes encoded in strains within the full consortium.

Enzyme	Species	Uniprot ID	% Identity	E-Value	Bit-Score	Strain
Phthalate 4,5-dioxygenase oxygenase reductase	<i>Pseudomonas</i> sp. 58R3	A0A1B5EAD8	81.65	0.00	541	10/13.2
Phthalate 4,5-dioxygenase	<i>Pseudomonas fulva</i> strain 12-X	F6AJ53	64.67	$1.82 \times 10^{-147}$	416	10/13.2
Ferredoxin	<i>Burkholderia cepacia</i>	A0A1Z3YX76	57.05	$2.73 \times 10^{-128}$	367	9.2/10/13.2
Reductase component of isophthalate dioxygenase	<i>Comamonas</i> sp. E6	C4TNS5	54.05	$2.47 \times 10^{-5}$	43.1	all
Putative phthalate dioxygenase reductase	<i>Acinetobacter johnsonii</i> SH046	D0SH70	51.43	$4.11 \times 10^{-114}$	330	10/13.2
Phthalate 4,5-dioxygenase	<i>Hydrogenophaga</i> sp. PBC	A0A1C9VA35	48.15	$1.09 \times 10^{-5}$	45.4	9.2
Phthalate-dioxygenase	<i>Hydrogenophaga intermedia</i>	A0A1L1P942	48.15	$1.09 \times 10^{-5}$	45.4	9.2/10/13.2
4,5-dihydroxyphthalatedecarboxylase	<i>Bacillus aquimaris</i>	A0A1J6W284	46.43	$1.42 \times 10^{-11}$	64.7	9.1
4,5-dihydroxyphthalatedecarboxylase	<i>Sporosarcina</i> sp. P17b	A0A2G5XE92	44.90	$2.82 \times 10^{-5}$	43.1	13.1
4,5-dihydroxyphthalatedecarboxylase	<i>Caballeronia megalochromosomata</i>	A0A149R8D0	44.00	$7.82 \times 10^{-5}$	41.6	9.2
Phthalate 4,5-dioxygenase oxygenase subunit	<i>Novosphingobium</i> sp. MBES04	A0A0S6WTD6	43.93	$2.44 \times 10^{-82}$	250	10/13.2
Phthalate 4,5-dioxygenase oxygenase reductase	<i>Bordetella pertussis</i> H921	A0A0N2IN58	43.66	$9.27 \times 10^{-7}$	47.4	9.2
Putative phthalate dioxygenase reductase	<i>Bordetella pertussis</i> H921	Q2YM46	43.66	$9.27 \times 10^{-7}$	47.4	9.2
Phthalate dioxygenase reductase	<i>Pandoraea sputorum</i>	A0A239SNB1	43.28	$5.05 \times 10^{-8}$	51.6	9.2
Aromatic ring-opening dioxygenase LigA	<i>Azoarcus</i> sp. PA01	A0A0M0FSY9	43.09	$2.04 \times 10^{-46}$	154	all
Extradiol ring-cleavage dioxygenase	<i>Gordonia phthalatica</i>	A0A0N9NE56	43.03	$4.80 \times 10^{-51}$	166	all
Putative phthalate dioxygenase reductase	<i>Brucella abortus</i> strain 2308	Q2YM46	42.82	$2.26 \times 10^{-102}$	305	9.2
Phthalate 4,5-dioxygenase (Phthalate dioxygenase)	<i>Ramlibacter tataouinensis</i>	F5XWD6	41.96	$5.06 \times 10^{-27}$	109	all
Phthalate 4,5-dioxygenase oxygenase (OhpA2)	<i>Paraburkholderia xenovorans</i>	Q13QM0	41.82	$8.89 \times 10^{-32}$	122	all
Phthalate 4,5-dioxygenase	<i>Mycolicibacterium wolinskyi</i>	A0A1X2FHI8	40.74	$4.99 \times 10^{-8}$	52	9.1/13.1
Phthalate 4,5-dioxygenase oxygenase (OhpA2)	<i>Variovorax</i> sp. WDL1	A0A109CIC4	39.54	$1.06 \times 10^{-4}$	37.7	9.1/10/13.1/13.2
Phthalate 3,4-dioxygenase alpha subunit	<i>Klenkia soli</i>	A0A1H0Q6Z9	38.89	$1.89 \times 10^{-11}$	62.4	13.1
Phthalate 4,5-dioxygenase oxygenase reductase	<i>Gibberella fujikuroi</i>	A0A0I9YA52	38.73	$2.29 \times 10^{-22}$	92.4	9.1/13.1
Ferredoxin	<i>Brevirhabdus pacifica</i>	A0A1U7DHI8	38.21	$1.30 \times 10^{-9}$	57	9.1/13.1
Phthalate 3,4-dioxygenase alpha subunit	<i>Rhodococcus</i> sp. OK302	A0A235G3V7	38.18	$2.65 \times 10^{-4}$	38.5	9.1/13.1
Oxygenase large subunit of phthalate dioxygenase	<i>Terrabacter</i> sp. strain DBF63	Q8GI63	38.18	$8.64 \times 10^{-4}$	37	all
Phthalate 4,5-dioxygenase oxygenase subunit	<i>Thalassobius gelatinovorans</i>	A0A0P1FRT5	37.84	$5.95 \times 10^{-20}$	82.8	13.1
4,5-dihydroxyphthalate decarboxylase	<i>Pseudoruegeria lutimaris</i>	A0A1G9AEN9	37.50	$9.18 \times 10^{-5}$	41.6	10/13.2
Phthalate dioxygenase reductase	<i>Gibberella subglutinans</i>	A0A109QSZ1	37.27	$1.64 \times 10^{-26}$	104	9.1
Phthalate 4,5-dioxygenase oxygenase subunit	<i>Alphaproteobacteria bacterium</i>	A0A2S6QA16	36.84	$4.36 \times 10^{-4}$	35.8	9.1
Phthalate 3,4-dioxygenase alpha subunit	<i>Mycolicibacterium rutilum</i>	A0A1H6J828	35.48	$7.71 \times 10^{-6}$	45.4	9.2
Oxygenase component of isophthalate dioxygenase	<i>Comamonas</i> sp. E6	C4TNS2	34.43	$1.37 \times 10^{-28}$	113	9.2/10/13.1/13.2
Putative phthalate dioxygenase reductase	<i>Providencia californiensis</i> PAL-3	W3YHJ5	33.64	$6.31 \times 10^{-9}$	54.7	9.1/13.1
3,4-dihydroxyphthalatedecarboxylase	<i>Arthrobacter</i> sp. strain FB24	A0AWN5	33.49	$2.26 \times 10^{-17}$	75.9	9.1/13.1
3,4-dihydroxy-3,4-dihydrophthalate dehydrogenase	<i>Terrabacter</i> sp. strain DBF63	Q8GI60	33.15	$2.80 \times 10^{-8}$	51.6	all
3,4-dihydroxyphthalatedecarboxylase	<i>Nocardioides terrae</i>	A0A1I1EG61	33.15	$3.34 \times 10^{-17}$	76.6	10/13.2
3,4-dihydroxyphthalatedecarboxylase	<i>Klenkia soli</i>	A0A1H0Q8Z1	32.52	$1.20 \times 10^{-14}$	69.3	9.2
Phthalate-dioxygenase	<i>Bradyrhizobium</i> sp. ORS3257	A0A2U3Q6T0	32.22	$1.48 \times 10^{-23}$	97.8	13.1
Cis-phthalate dihydrodiol dehydrogenase	<i>Comamonas</i> sp. E6	A0A0M2DHI3	31.90	$2.50 \times 10^{-18}$	82.8	9.2
Phthalate 3,4-dioxygenase alpha subunit	<i>Rhodococcus rhodnii</i> LMG5362	R7WIP7	31.63	$1.31 \times 10^{-38}$	140	10/13.2
Cis-phthalate dihydrodiol dehydrogenase	<i>Burkholderia multivorans</i>	A0A0H3KKN4	28.89	$2.13 \times 10^{-8}$	52.8	9.1/10/13.1/13.2

## 2.7. Strains within the Full Consortium Have Diverse Carbon Sources Utilization

A microbial community-based analysis was performed using Biolog EcoPlates® to assess the overall carbon utilization amongst the strains and the full consortium. Results indicate a wide substrate capability (Figure 5) of the individual strains, which is also evidenced by their pangenomes (Figure 1).

The non-aromatic amino acid L-asparagine was the preferred carbon source of most strains, and as a result, this carbon source was chosen as a control for further transcriptomic analysis of PET degradation. Of the most interest, as examined above, was the paraben 4-hydroxybenzoic acid, which was within the top ten fastest utilized carbon sources for the full consortium. This carbon source is proven to be transported into the cell using PcaK [54,55] and is hypothesized to be a probable transporter for TPA in the *Pseudomonas* species.

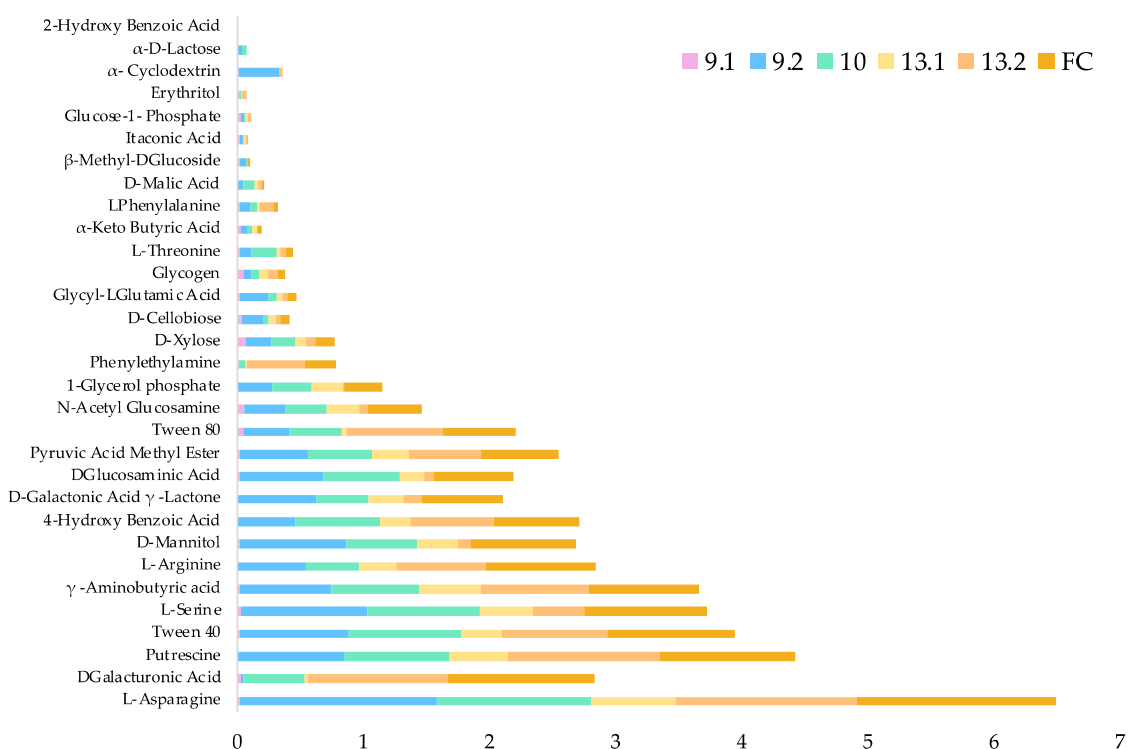


**Figure 5.** Comparison of relative carbon source utilization between the individual strains and the full consortium over 24-h using Biolog EcoPlates<sup>®</sup>. Thirty-one carbon sources, in triplicate, were evaluated kinetically via a colorimetric assay over a 24-h period at room temperature ( $25 \pm 2$  °C). Triplicate values were averaged to determine relative absorbance compared to the control samples (water).

As expected, based on previous screenings [25] for lipase and esterase activity, Tween 40 was a favorable carbon source amongst the strains. Overall, amino acids and other nitrogen-containing compounds tended to be a favorable carbon source for all strains, excluding *Bacillus* 9.1. Strain 9.1 was -growing under room temperature conditions and preferentially grew on polysaccharides and monosaccharides, as well as the chitin monomer, N-acetyl-glucosamine, and non-ionic surfactant Tween 80. This slow growth may be temperature-dependent, as *Bacillus* 9.1 grows rapidly at 40 °C. Putrescine was also preferred by the full consortium, which is of interest, as putrescine is an alkane. This provides further evidence there that the full consortium may possess alkane metabolism potentially involved in LDPE degradation [56,57].

In contrast to the observed synergy on PET, the full consortium did not degrade as wide of a range of substrates as the individual strains (with the exception of *Bacillus* strain 9.1, 77%) with a functional diversity score of 84% (see methods for diversity and similarity scoring); however, the full consortium did utilize preferred carbon sources more efficiently than all other strains, reaching an average optical density greater than the individual strains in the same time period (Supplemental Table S1) despite the same inoculation concentration and conditions. *Bacillus* strain 13.1 and the full consortium were the most similar in carbon source utilization, with 90% similarity. *Pseudomonas* strain 10 had the most diverse carbon utilization of all, with a 97% functional diversity, able to utilize all but 2-hydroxy benzoic acid. Despite *Pseudomonas* 10 and 13.2 being the same species, they were only 90% similar in carbon source utilization. This stark contrast in carbon source utilization and the differences within the pangenome (Figure 1) show incredible functional genetic diversity.

These differences might explain the observed variations in growth and biofilm formation (Figure 6). Using a crystal violet microtiter assay, differences in biofilm formation between individual strains and the full consortium were quantified. *Pseudomonas* strains 9.2 and 10 exhibited significantly more biofilm formation than strains 9.1, 13.1, 13.2, and

the full consortium. Of greatest interest was the difference in biofilm production between *Pseudomonas* strains 10 and 13.2, which are the same species. After 48 h of growth at 37 °C, strain 10 exhibited a solubilized crystal violet optical density of  $0.12 \pm 0.035$ , while the optical density of strain 13.2 was only  $0.03 \pm 0.015$ . This significant difference could perhaps be attributed to the two strains' variation in carbon source utilization, their differences in transcriptional activity, and their distinct species-specific pangenome encode proteins.

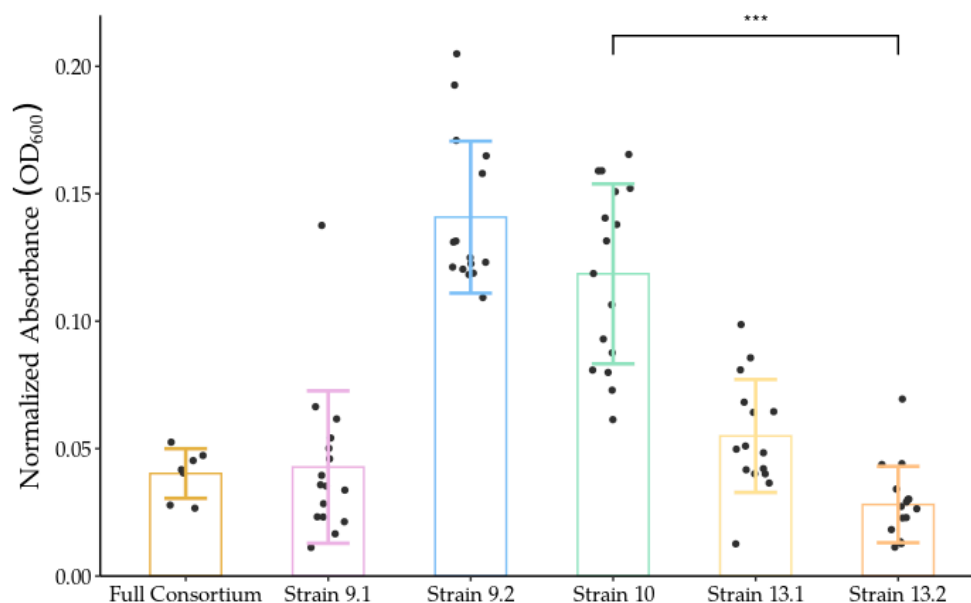


**Figure 6.** Quantification of biofilm production using crystal violet stain. Comparison of biofilm formation between the individual strains and the full consortium grown for 48 h on polystyrene 96-well plates. Biofilm production was quantified, minus background absorbance, by measuring optical density of biofilms stained with crystal violet at 600 nm using a TECAN infinite 200. \*\*\*  $p < 0.0001$ . Error bars denote one standard deviation from the mean.

### 2.8. Differential RNAseq Analysis Shows Diverse Transcriptional Activity Amongst the Individual Strains Related to PET Monomer Degradation and PHA Storage

RNA sequencing (RNAseq) analysis provided insight into how the full consortium may be interacting and metabolizing PET and its monomers during the late exponential phase of growth. It appears the strains within the full consortium may be degrading PET in different ways, possibly explaining synergistic effects. Differential analysis obtained by using data from the full consortium grown on L-asparagine as a control compared to PET indicates a significant upregulation of genes related to initial PET degradation; the predicted monomer metabolism of both TPA and EG, as well as downstream PHA metabolism, were also observed to be upregulated amongst the strains (Table 4).

A previous transcriptomic analysis from Kumari et al. [35], proposed that aldehyde dehydrogenases are active against PET in *Bacillus*, generating 4-[(2-hydroxyethoxy)carbonyl] benzoate resulting from the deprotonation of the free carboxy group of MHET. In this study, RNAseq analysis of the full consortium grown on PET has shown a significant upregulation of an aldehyde dehydrogenase in strain 9.2. This aldehyde dehydrogenase might be acting on EG but may also act on PET itself. As EstB was also experimentally shown to hydrolyze PET to MHET, this further supports the work of Kumari et al., who proposed that aldehyde dehydrogenases and carboxylesterases play a role in PET hydrolysis in some species [35].

Despite TPA degradation-related genes being absent in strain 9.1 [25] during previous genome exploration, based on differential analysis and annotation, strain 9.1 had significant upregulation of genes with significant identity to phthalate dioxygenases and dehydrogenase (Table 4), as well as a phenol hydrolase. A transporter with significant identity to a gentisate transporter (GenK) was also upregulated and is likely how TPA or oligomers

of PET may transverse the outer membrane of strain 9.1. Additionally, in 9.1, an alcohol dehydrogenase and a glyoxal reductase were upregulated, likely illustrating its role in ethylene glycol metabolism.

**Table 4.** Differential expression of upregulated genes within the individual strains that may be involved in PET degradation.

Strain	Gene	logFC	logCPM	p-Value
9.1	Poly(3-hydroxyalkanoate) depolymerase	3.42	2.09	$3.64 \times 10^{-2}$
	Phthalate 4,5-dioxygenase, reductase subunit	2.60	8.24	$2.20 \times 10^{-9}$
	Short-chain dehydrogenase/reductase	1.90	3.59	$6.32 \times 10^{-3}$
	Alcohol dehydrogenase 2	1.47	3.50	$3.79 \times 10^{-2}$
	Poly(3-hydroxyalkanoate) depolymerase	1.35	10.69	$4.09 \times 10^{-3}$
	Phenol hydrolase	1.31	10.94	$1.68 \times 10^{-4}$
	Poly(3-hydroxybutyrate) depolymerase	1.14	12.18	$8.31 \times 10^{-4}$
	Glyoxal reductase	0.89	7.14	$1.58 \times 10^{-2}$
	Gentisate transporter	0.70	9.60	$4.30 \times 10^{-2}$
9.2	Taurine dioxygenase	3.67	2.06	$4.91 \times 10^{-3}$
	Putative regulatory protein	2.90	2.32	$1.75 \times 10^{-2}$
	Short-chain dehydrogenase/reductase	1.21	5.19	$2.51 \times 10^{-2}$
	Beta-carboxy-cis,cis-muconate cycloisomerase	1.05	10.95	$2.52 \times 10^{-3}$
	Beta-ketoadipyl CoA thiolase	0.97	8.61	$1.10 \times 10^{-2}$
	Aldehyde dehydrogenase	0.89	8.35	$3.30 \times 10^{-2}$
	Poly(3-hydroxyalkanoate) depolymerase	0.78	9.45	$3.32 \times 10^{-2}$
10	Poly(3-hydroxybutyrate) depolymerase	2.80	-0.54	$3.93 \times 10^{-3}$
	3,4-dihydroxyphthalate decarboxylase	2.48	7.72	$2.19 \times 10^{-8}$
	Terephthalate 1,2-dioxygenase, oxygenase	1.32	1.20	$3.09 \times 10^{-2}$
	Putative regulatory protein	1.19	6.38	$4.34 \times 10^{-4}$
	Putative regulatory protein	1.09	5.72	$9.15 \times 10^{-4}$
	4,5-dihydroxyphthalate decarboxylase	1.07	5.63	$8.44 \times 10^{-4}$
	Poly(3-hydroxybutyrate) depolymerase ( <i>nlhH</i> )	1.04	5.15	$2.35 \times 10^{-3}$
	Beta-carboxy-cis,cis-muconate cycloisomerase	0.84	9.74	$7.32 \times 10^{-3}$
	Putative regulatory protein	0.78	9.89	$3.17 \times 10^{-2}$
	Poly(3-hydroxybutyrate) depolymerase	0.74	10.89	$1.74 \times 10^{-2}$
	Quercetin 2,3-dioxygenase	0.68	6.18	$3.37 \times 10^{-2}$
Surfactin synthase subunit 3	1.03	4.21	$4.71 \times 10^{-3}$	
13.2	Poly(3-hydroxybutyrate) depolymerase	2.80	-0.54	$3.89 \times 10^{-3}$
	3,4-dihydroxyphthalate decarboxylase	2.48	7.72	$2.11 \times 10^{-8}$
	Terephthalate 1,2-dioxygenase, terminal oxygenase	1.32	1.20	$3.09 \times 10^{-2}$
	Putative regulatory protein	1.23	5.24	$2.26 \times 10^{-3}$
	Putative regulatory protein	1.19	6.38	$4.31 \times 10^{-4}$
	Poly(3-hydroxybutyrate) depolymerase ( <i>nlhH</i> )	1.13	5.11	$8.26 \times 10^{-4}$
	Beta-carboxy-cis,cis-muconate cycloisomerase	0.84	9.74	$7.31 \times 10^{-3}$
	Putative regulatory protein	0.78	9.89	$3.14 \times 10^{-2}$
	Poly(3-hydroxybutyrate) depolymerase	0.74	10.90	$1.73 \times 10^{-2}$
	Poly(3-hydroxyalkanoate) depolymerase	0.73	8.09	$2.62 \times 10^{-2}$
	Quercetin 2,3-dioxygenase	0.68	6.18	$3.32 \times 10^{-2}$

A differential analysis of RNAseq transcripts from strain 10 and 13.2 suggests TPA was actively being degraded at the time of RNA extraction. Numerous dioxygenases and decarboxylases with significant identity to phthalate oxidoreductases, including Terephthalate 1,2-dioxygenase, were present (Table 4). Additionally, evidence of downstream beta-ketoadipate metabolism indicates that TPA is being further metabolized, likely toward PHA/PHB synthesis.

The upregulation of related genes and PHA biosynthesis were present in all strain transcripts (Table 4). Both *Pseudomonas* strains 10 and 13.2 had significant transcriptional upregulation of carboxylesterase NlhH, which was identified within the pangenome above as likely a PHA/PHB depolymerase [58]. The deletion of *nlhH* in strain 9.2 showed no reduction of np-butyrate hydrolysis (Supplemental Figure S3), indicating differences in esterase activity compared to EstB and may or may not be directly involved in PET polymer depolymerization.

Interestingly, only strain 10 had an increased transcription level of surfactin (Table 4), and 113 ‘hypothetical proteins’ were upregulated in strain 10, whereas only 77 were upregulated in strain 13.2 (Supplemental File S4). These gene differences in strain 10 may partially explain the differences in biofilm production [59] (Figure 6).

### 3. Discussion

By using the pangenome of the full consortium containing three *Pseudomonas* and two *Bacillus* strains, we were able to predict which enzymes were potential PET degradation enzymes. From this analysis, many hydrolases, oxidoreductases, and dehydrogenases were identified (Supplemental File S3). Previously, a group determined that a secreted carboxylesterase 2, EstB encoded in *Enterobacter* sp. HY1, was able to degrade BHET, a monomer of PET [39]. As our group identified an EstB within the pangenome, we hypothesized this enzyme within the *Pseudomonas* strains might be a PET/BHET hydrolyzing enzyme. After screening for p-np-butyrate esterase activity via the deletion and purification of EstB (Figure 2), as well as incubation on BHET and PET, our data indicated that EstB hydrolyzed BHET to the oligomer MHET and the monomer TPA (Figure 3), similar to the *Ideonella sakaiensis* PETase [16].

A comparison of the structure of *IsPETase* [60] to the predicted structure of EstB revealed considerable structural similarity, including a similar binding cleft, catalytic triad, and lack of a lid structure (Figure 4), indicating that EstB is a PETase. The observations of similar active sites and enzymatic activities, combined with a relatively low primary amino acid sequence identity between the *IsPETase* and EstB, is consistent with the idea of the convergent evolution of bacteria in disparate locations to evolve the ability to degrade PET and other plastics. EstB was predicted to have feruloyl esterase activity when aligned with the PMBD (Table 1), and other enzymes that could potentially degrade PET were also identified.

The predicted PETases included two diene lactone hydrolases encoded in both *Pseudomonas* strains 10 and 13.2 and in *Bacillus* strain 9.1. Further transcriptomic analysis within the *Pseudomonas* strains indicated the upregulation of carboxylesterases NlhH in strains 10 and 13.2 and an aldehyde dehydrogenase upregulated in 9.2 (Table 4) when the strains were incubated on PET. Kumari et al. previously identified, through transcriptomic analysis, the complex interactions of carboxylesterases and aldehyde dehydrogenases on the degradation of PET, possibly through the generation of 4-[(2-hydroxyethoxy) carbonyl] [35]. This study gives further evidence of potential aldehyde dehydrogenase- and carboxylesterase-mediated PET degradation.

While the *Pseudomonas* strains seemed to be actively metabolizing PET and TPA using the presence of various oxidoreductases and dehydrogenases (Table 4), *Bacillus* strain 9.1 seems to play a key role in ethylene glycol metabolism. Strain 9.1 had a high upregulation of an alcohol dehydrogenase and glyoxalase, which are two genes implicated in EG metabolism. However, strain 9.1 also might be involved in BHET and TPA metabolism. The upregulation of the aromatic transporters GenK in *Bacillus* strain 9.1 may be responsible for PET monomer uptake, such as TPA. The downstream metabolism of TPA was observed within the *Pseudomonas* species via the presence of genes involving Beta-ketoadipate, butonate, and polyhydroxyalkanoate (PHA) metabolism.

It is likely the consortia utilize stored biopolymers PHA/PHB as a supplementary carbon source over time. After hydrolyzing the PET polymer and oligomers, PET monomers are assimilated, and the consortia generate biopolymer PHA. Evidence of PHA synthesis and depolymerization is shown in the upregulation of PHA/PHB depolymerases and synthases (Table 4) when grown on PET. It is hypothesized that there is an inability to cleave PET further after reaching the late exponential/stationary phase, either through the buildup of toxic intermediaries or product inhibition. This storage of PHA/PHB provides potential “upcycling” of PET waste as an alternative biodegradable plastic.

One important aspect of PET degradation is the ability of the bacteria to adhere to the surface of the hydrophobic polymer. Biofilms are crucial for PET degradation due to

increased adherence to the surface of PET, accompanied by increased hydrophilicity and carbonyl index [61]. Biofilm production was measured in all consortia members (Figure 6), and the data indicated that *Pseudomonas* strain 10 possessed the greatest biofilm potential, compared to the other strains. Surfactin production directly results in increased biofilm formation [59], and we observed the presence of and significant upregulation of surfactin in strain 10, which is consistent with the increased biofilm formation capabilities. This was not observed in *Pseudomonas* strain 13.2 or the other consortium members.

The transcripts between all strains, particularly *Pseudomonas* 10 and 13.2, that were grown on plastic varied dramatically. Interestingly, strain 10 contained 70 unique species-specific hypothetical proteins different from the pangenome, while 13.2 contained 58, even though they are genetically the same species. This might, in part, explain the observed differences in growth and gene expression (Table 4) and biofilm formation (Figure 6). These data provide insight into how the consortia might be interacting when grown on the surface of PET, showing different functional roles. Of note, *Bacillus* strain 13.1 had very few transcripts, possibly indicating a temporal function in early phases of PET biodegradation but not in later stages.

While able to degrade PET, this environmental consortium is also highly carbon diverse; the strains are able to degrade a wide variety of carbon sources, illustrated by the Biolog EcoPlate data (Figure 5) and the large number of predicted polymer biodegradation genes (Tables 1 and 2). The full consortium appears to have a pangenome capable of degrading a variety of plastic types, which would make mixed plastic recycling possible. Polyurethane [24], LDPE [62,63] and PLA [64,65] degradation have been observed by both *Pseudomonas* and *Bacillus* spp. previously. PVA, a water-soluble plastic that is typically used in dish and laundry detergent “pods” and has been entering waterways and ecosystems due to unprecedented commercial use [66,67], was also predicted to be degradable by the full consortium.

Importantly, not only do these strains contain predicted genes capable of degrading multiple plastic types, but they are also predicted to degrade common plasticizers, including phthalates, paraben, and other aromatic/phenolic compounds. These plasticizers leach and are ecotoxic, unlike most inert plastics [68]. This illustrates the capability of consortia to degrade mixed plastic types, including those with certain additives. Plasticizers are crucial in the discussion of plastic wastes, as they leach over time [69,70] and are of concern, as research has shown them to be acutely toxic to humans and the environment [71–73]. Additives have historically been largely unregulated [74], and many are not required to be disclosed or labeled. While certain additives have shown to be biodegradable [75], many are not, as many products seek to be anti-microbial.

These plasticizers pose challenges for not only biological recycling efforts but also for conventional chemical and mechanical recycling, as they limit how many times a plastic can be recycled, if at all [74]. Even though microorganisms are slowly and globally utilizing plastics as a carbon source, without a collaborative effort, the plastic pollution problem will only worsen. Luckily, some efforts to increase the regulation of and research into plasticizers are ongoing [76]. Research surrounding plasticizers’ environmental toxicity and biodegradability, if intended to be part of single-use products, should be fully considered. With the proper governmental regulation of non-toxic plastic additives amenable to biodegradation [75], it is possible to pursue biological consortia-based approaches toward plastic recycling and bio-upcycling efforts.

## 4. Materials and Methods

### 4.1. Omics Approaches

#### 4.1.1. Pangenome Analysis

Genomes deposited in GenBank (BioProject Accession: PRJNA517285) were uploaded to the MicroScope (LABGeM, Courcouronnes, FRA) [37] website for expert annotation and comparative genomic analysis using the Pan-genome Analysis tool. Pangenomes and core/variable genomes were generated using MicroScope gene families (MICFAM)

computed using SiLiX software [38]. MICFAM parameters were set to 50% aa identity/80% alignment coverage. The core genomes of 232 genomes (i.e., all *Pseudomonas* (144) and *Bacillus* (88) species, within the MicroScope platform database (excluding the five strains within the full consortium) at the time of this analysis) were excluded from the analysis. Supplemental Figure S1 contains a phylogram of all species included in the analysis.

#### 4.1.2. PMBD Analysis

The PMBD database is comprised of 949 microorganisms with 79 genes indicated in the biodegradation of plastics and more than 8000 annotated enzymes/proteins predicted to be involved in plastics biodegradation [36]. The annotated pangenomes of all five strains within the full consortium were obtained from the MicroScope platform [37]. These sequences were BLASTED against the PMBD database; e-value cutoff >0.001 and sequences with greater than 20% percent identity were considered significant alignments.

### 4.2. RNA Sequencing to Determine Genes Implicated in PET Biodegradation

#### 4.2.1. Total RNA Extraction and Sequencing

Bacterial cultures of the full consortium were prepared in Liquid Carbon Free Media (LCFBM) as published [25] with either 1% (*w/v*) granular PET or L-asparagine. Optical Density measurements at 600 nm (OD<sub>600</sub>) were used to determine when the culture had reached mid to late exponential phase of growth. L-asparagine was harvested after reaching exponential phase at an OD<sub>600</sub> of 0.300 A, and the PET samples were harvested once they reached an optical density of 0.200 A. Cells were pelleted and resuspended in RNAProtect bacteria reagent (Qiagen, Germantown, MD, USA) to prevent RNA degradation and frozen at −80 °C until time of extraction.

As extraction of total RNA from mixed culture of bacteria may present bias against species within the culture, RNA extraction was conducted according to the GTC method and DNA removal previously described by Stark et al. 2014 for the most efficient extraction rate for both *Bacillus* and *Pseudomonas* [77]. All chemicals required were purchased from Sigma-Aldrich (Sigma-Aldrich, St. Louis, MO, USA). Total RNA extractions were tested for purity and quantity using a Nanodrop™ 1000 Spectrophotometer (Thermo Fisher Waltham, MA, USA) and Qubit™ 4 Fluorometer (Invitrogen, Waltham, MA, USA). Illumina prokaryotic RNA sequencing was completed by Novogene Beijing Bioinformatics Technology, Co., Ltd. Illumina NovaSeq 6000 (Novogene, Beijing, CHN).

#### 4.2.2. RNAseq Analysis

Paired-end Illumina RNA sequences were generated for two control and two experimental samples. The quality of the raw reads was assessed with FastQC v0.11.3 [78]. After QC v0.9.6 was run to separate and retain high-quality sequences [79], high-quality transcripts were then used to recruit onto each individual genome within the consortium using Bowtie2 v2.3.5.1 [80]. SAM files were generated using Samtools v1.10 [81]. Expression was calculated and normalized using FeatureCounts v2.0.1 [82]. Once expression was calculated, differential expression between the control and the experimental treatments was calculated using the Bioconductor/R packages DESeq2 v1.34.0 and EdgeR v3.36.9 [83,84]. Upregulated genes for each individual genome were analyzed at a cut-off e-value of 0.05. Specific genes/enzymes associated with PET degradation were selected if they were upregulated in relation to the control.

### 4.3. Evaluation of Carbon Source Utilization and Strain Biofilm Production

#### 4.3.1. Biolog EcoPlates

The growth of overnight bacterial cultures grown in LB was measured via OD<sub>600</sub>. They were rinsed as previously described [25] and diluted to 0.1 A before their addition to each plate. Observance of purple color was indicative of respiration, as the cells reduce the tetrazolium dye included within each carbon source in the plate. Thirty-one carbon sources, in triplicate, were evaluated kinetically according to the manufacturer's instruction

(Biolog EcoPlate, Hayward, CA, USA) using a colorimetric assay (clear to purple, OD<sub>590</sub>) via a Tecan infinite M200PRO microplate reader (Tecan, Zürich, CHE) over a 24-h period (over 80,000 s) at room temperature (25 ± 2 °C). Triplicate values were averaged in Excel (Microsoft Corporation, Redmond, WA, USA) analysis of relative absorbance for each sample over time, which was determined via subtraction of the control (water) to account for spontaneous tetrazolium dye formation.

To examine quantitative relationships between the strains and their ability to utilize the 31 unique carbon sources, two calculations were performed to determine the functional diversity based on all 31 carbon sources and the strain's/consortium's relative similarity (Ssm).

$$\% \text{ Functional Diversity} = (a \div 31) \times 100.$$

$$\% \text{ Similarity (Ssm)} = ((a + d) \div (a + b + c + d)) \times 100.$$

a = the number of carbon sources used by strains and consortia.

b = the number of carbon sources used the strain of interest only.

c = the number of carbon sources used by the full consortium/other strain only.

d = the number of carbon sources not utilized by either.

#### 4.3.2. Microtiter Plate Biofilm Quantification Assay

Growth of overnight bacterial cultures for individual strains incubated in LB at 26 °C was measured via OD<sub>600</sub>. Cells were rinsed, followed by dilution in M63 media to OD<sub>600</sub> = 1. A suspension of the full consortium was created by combining equal volumes of the five individual strain suspensions. These suspensions were further diluted to 1:100 in M63 supplemented with 0.2% ethanol, 1 mM MgSO<sub>4</sub>, and 0.5% casamino acids and transferred to a polystyrene FALCON non-tissue culture treated microtiter plate (Corning, Corning, New York, USA) (100 µL/well). Negative controls consisted of supplemented M63 only. After 48 h of incubation at 26 °C, planktonic growth was removed, and the wells were gently washed with 125 µL of sterile phosphate-buffered saline (PBS). Biofilms were stained with 0.1% crystal violet (125 µL/well) for 15 min and then washed three times with 125 µL PBS. The remaining dye was solubilized with 100% ethanol (200 µL/well) for 15 min, then 100 µL/well was transferred to a new polystyrene microtiter plate. The optical density of solution in each well was measured at 600 nm using a microplate reader (Infinite 200, TECAN, Grödig, Salzburg, AUT).

#### 4.4. Mutant Preparation of *ΔestB*

Single gene deletion of *estB* in *Pseudomonas* strain 9.2 was performed as previously described [40]. Briefly, primers were designed to amplify fragments upstream and downstream of *estB* (upstream forward, 5'-ccgggtaccgagctcgaattCACGATCGCCAGAGTGGATT-3' and upstream reverse, 5'-ggcgaccctgtcgcaattgGGCTGCTCCAATTGTGTGCG-3'; downstream forward, 5'-cgcacacaattggagcagccCAATTGCGACAGGGGTCGCC-3' and downstream reverse, 5'-tatgaccatgattacgaattTAACCCAGCACCTGAGCCTG-3', uppercase indicates annealing segment). These primers contain overhang segments to facilitate ligation into the vector *pEX18Tc* using an NEB Gibson Assembly kit (New England Biolabs, Ipswich, MA, USA). Correct assembly of the vector was confirmed by amplifying the MCS using *pEX18Tc* universal primers (forward, 5'-GGCTCGTATGTTGTGTGGAATTGTG-3' and reverse, 5'-GGATGTGCTGCAAGGCGATTAAG-3') and sequencing that fragment (ACGT Sequencing, Wheeling, IL, USA). Assembled vector with flanking *estB* fragments (*pRDEXestB*) was transformed into *Pseudomonas* strain 9.2, and merodiploids were selected by growth on LB-tetracycline (15 µg/mL). Deletion of *estB* was induced by growing merodiploids of sucrose plates (TYS10) and was confirmed by amplifying and sequencing a fragment spanning slightly upstream and downstream of *estB* (forward, 5'-CGCTGACACCCAGTACTGCAGC-3' and reverse, 5'-GATCGAGATCAGGAACGCGGCG-3'). All PCR conducted utilized a touchdown protocol with Q5 polymerase.

#### 4.5. EstB Purification

##### 4.5.1. Amplification and Purification of estB Vector Insert

Primers were designed using Benchling (Benchling, San Francisco, CA, USA) to amplify estB without its start or stop codon in order to express EstB with a C-terminal T7 tag and an N-terminus 6xHis tag. These designed primers included partial overhangs to allow for assembly into the expression vector. The primers are as follows: forward, 5'-atgggtcgcggatccgaattGACCGAGCCCTTGATTCTTCAGCCC-3', reverse, 5'-ttgtcgcaggagctcgaattGCGCAGGCGTTCGCTCAACCAT-3' (uppercase characters indicates annealing segment). PCR was performed using genomic DNA obtained by incubating one colony of *Pseudomonas* strain 9.2 in 100 µL DNase-free water at 100 °C for 5 min (2 µL of this solution was used for a 20 µL PCR reaction). Each PCR contained 0.5 µM of forward and reverse primers, 200 µM dNTPs, 1× Q5 high GC enhancer, and 0.02 U/µL Q5 DNA polymerase in a 1× Q5 reaction buffer (New England Biolabs, Ipswich, MA). The thermocycler was programmed with a touchdown PCR protocol as follows: 98 °C for 1 min, 16 cycles of 98 °C for 10 s, 68 °C for 30 s with a 0.5 °C decrease every cycle, 72 °C for 20 s, followed by 30 cycles of 98 °C for 10 s, 60 °C for 30 s, 72 °C for 20 s, followed by a final extension of 72 °C for 2 min. Fragments were confirmed through gel electrophoresis and extracted and purified using a gel extraction kit (QIAGEN, Germantown, MD, USA).

##### 4.5.2. Assembly, Isolation, and Purification of RDpET24estB Expression Vector

The expression vector pET-24a(+) was linear by restriction digest with EcoRI. Gibson assembly was performed using reagents from NEB Gibson Assembly Cloning Kit. The reaction mix contained 1× Gibson master mix and a 4:1 molar ratio of insert to linearized plasmid (0.116 pmol estB insert and 0.029 pmol linearized pET-24a(+) vector). The reaction mixture was incubated at 50 °C for 15 min, then transformed into NEB 5-alpha *E. coli* via heat shock and plated on LB-kanamycin agar media. Transformants were inoculated in LB-kanamycin media, and plasmid DNA was extracted using a QIAGEN plasmid isolation kit. PCR was performed on both the transformant and the purified plasmid to confirm that the vector was correctly assembled. The primers used are the T7 universal primers for the pET-24a(+) vector: forward, 5'-TAATAACGACTCACTAATAGG-3', reverse, 5'-GCTAGTTATTGCTCAGCGG-3'. PCR was performed using either genomic DNA obtained by incubating one colony of NEB 5-alpha *E. coli* in 100 µL DNase-free water at 100 °C for 5 min (2 µL of this solution was used for a 20 µL PCR reaction) or 10 ng of purified plasmid. Each PCR contained 0.5 µM of forward and reverse primers, 200 µM dNTPs, 1× Q5 high GC enhancer, 0.02 U/µL Q5 DNA polymerase in a 1× Q5 reaction buffer. The thermocycler was programmed with a touchdown PCR protocol as follows: 98 °C for 1 min, 10 cycles of 98 °C for 10 s, 60 °C for 30 s with a 1 °C decrease every cycle, 72 °C for 20 s, followed by 30 cycles of 98 °C for 10 s, 50 °C for 30 s, 72 °C for 20 s, followed by a final extension of 72 °C for 2 min. Fragments were confirmed through gel electrophoresis and purified using a QIAGEN PCR purification kit.

##### 4.5.3. Electroporation of BL21 *E. coli*

An overnight culture of BL21 *E. coli* (8 mL, OD<sub>600</sub> = 0.5) was pelleted by centrifugation (8000 rpm) for 10 min. Supernatant was discarded, and pellet was washed (3 × 1 mL ice-cold 10% glycerol) before being resuspended in 200 µL 10% glycerol. Roughly 0.5 µg of RDpET24estB vector was added to 50 µL cell suspension and incubated on ice for 1 min. Mixture was transferred to a pre-chilled electroporation cuvette and pulsed at 2.2 kV for 5.7 ms using a Bio-Rad MicroPulser (Bio-Rad, Hercules, CA, USA) before being transferred to 1 mL S.O.C. media and incubated in a 37 °C shaker for 1 h. Cells were plated on three individual LB agar plates containing 30 µg/mL kanamycin as follows: 50 and 100 µL of the solution, followed by pelleting the remaining solution via centrifugation (12,000 rpm) and reducing the total supernatant volume to 100 µL before resuspending the pellet and plating that solution. The plates were incubated at 37 °C overnight. Transformants were

confirmed by PCR and gel electrophoresis (procedure identical to the PCR performed in the previous section).

#### 4.5.4. Expression and Purification of EstB

Two flasks containing 250 mL LB media with 30 µg/mL kanamycin were inoculated with BL21 E. coli containing the RDpET24estB expression vector and were grown shaking at 37 °C to an OD<sub>600</sub> of 0.6. Once the desired OD<sub>600</sub> was achieved, IPTG was added to each flask to a concentration of 0.1 mM, and the cultures were grown shaking at 16 °C overnight. Cells were harvested by centrifugation (5000 rpm) at 4 °C, supernatant was discarded, and pellet was resuspended in 30 mL lysis buffer (50 mM NaPO<sub>4</sub>, 300 mM NaCl, pH 8). Half a cComplete™ protease inhibitor cocktail tablet (Roche, Mannheim, DEU) and lysozyme from chicken egg white (Sigma-Aldrich, St. Louis, MO, USA) to 0.4 mg/mL was added, and the mixture was incubated on ice for 20 min, vortexing frequently to ensure the protease tablet dissolved. Cells were lysed via sonication (6 × 10 s on, 20 s off, 70% power) before the solution was centrifuged (16,000 rpm) for 30 min at 4 °C. Roughly 10 mL of QIAGEN Ni-NTA agarose solution was pelleted by centrifugation (1600 rpm) for 5 min at 4 °C. Resin was allowed to settle for 5 min before discarding supernatant. The resin was washed (3 × 10 mL water, 1600 rpm centrifugation) before a final wash with 10 mL lysis buffer. Lysate was added to the resin and allowed to bind by gently shaking and inverting the tube for 1 h at 4 °C. Lysate-resin mixture was applied to a column and allowed to empty via gravity. Column was washed first with 5 × column volumes (CVs) of wash buffer A (50 mM NaPO<sub>4</sub>, 300 mM NaCl, 10 mM imidazole, pH 8), then 3 × CVs of wash buffer B (50 mM NaPO<sub>4</sub>, 300 mM NaCl, 20 mM imidazole, pH 8). Elution was done by adding a 3 × CVs elution buffer (50 mM NaPO<sub>4</sub>, 300 mM NaCl, 250 mM imidazole, pH 8). The flow-through from each CV added was collected in a different test tube and stored at 4 °C. Resin was washed 2 × CVs elution buffer, then 2 × CVs water, before being stored in 10 mL 20% ethanol at 4 °C. Purification of EstB was confirmed through SDS PAGE. Elutions containing only protein were pooled and dialyzed into 50 mM Tris-HCl, 150 mM NaCl, pH 8.0 buffer. Protein concentration was determined by measuring the absorbance at 280 nm with a NanoDrop-1000 (Thermo Fisher Waltham, MA, USA), and through a BCA Assay Kit (Thermo Fischer Scientific, Waltham, MA, USA). Aliquots of protein solutions in 25% glycerol and 1 mM DTT were stored at −20 °C.

#### 4.6. Screening Purified EstB and Mutant ΔestB for Esterase Activity

*Mutants:* Esterase activity was quantified based on the absorbance of 4-nitrophenol at 402 nm released from the hydrolysis of 4-nitrophenol butyrate [39]. The following reactions were performed in 200 µL volumes and in triplicate: just buffer (LCFBM), buffer with 4-nitrophenol butyrate (1.2 mM), and buffer with 4-nitrophenol butyrate and culture (1.2 mM, OD<sub>600</sub> = 0.1 in reaction volume). The microplate reader (Tecan) was set to 10 cycles of 30 min at room temperature and measuring absorbance at 402 nm.

*Enzyme:* Esterase activity was quantified based on the absorbance of 4-nitrophenol at 402 nm released from the hydrolysis of 4-nitrophenol butyrate. In a solution of acetonitrile:isopropanol (1:4 v/v) 4-nitrophenol butyrate (Sigma-Aldrich, St. Louis, MO, USA) was solubilized to 20 mM and stored at 4 °C. The following reaction conditions were performed in 200 µL reaction volumes in a clear 96-well plate (Corning, Corning, NY), with each reaction performed in triplicate: just buffer (50 mM HCl, 1 mM CaCl<sub>2</sub>, pH 7.5), buffer with 4-nitrophenol butyrate (1 mM), buffer with *estB* (5 nM), and buffer with 4-nitrophenol butyrate (1 mM) and *estB* (5 nM). Absorbance of each well was measured every min for 30 min at 402 nm by a microplate reader (Tecan).

#### 4.7. Screening for PET and BHET Degradation

##### 4.7.1. Synthesis of microPET and nanoPET

MicroPET was synthesized as outlined by Rodríguez-Hernández et al. [85] in order to increase the exposed surface area of the material and enhance degradation. Post-consumer

PET soda bottles (Coke and Pepsi) were cut into 1 cm strips of various lengths, discarding the caps and taking care to discard any labels. A total of 50 g of post-consumer PET strips were placed into a sterilized stainless steel blender (Waring Commercial, Stamford, CT, USA), and liquid N<sub>2</sub> was added until it fully covered the strips. The blender was set to high, and the liquid nitrogen was replaced until the PET was ground into a mixture of dust and small, jagged pieces. A total of 1 g of this ground PET mix was added to a beaker containing 10 mL of 90% (v/v) trifluoroacetic acid (TFA) and stirred for an hour until the PET was fully dissolved. Following the solvation of PET, 10 mL of 20% (v/v) TFA was added to the beaker and left overnight to let the PET crystallize out of solution. The mixture was then centrifuged at 6000 RCF (2496 G) for 1 h and the supernatant was discarded and replaced with 100 mL of a resuspension solution composed of 0.5% (w/w) sodium dodecyl sulfate. This mixture was ultrasonicated (5×, t = 10 s) via Misonix 3000 sonicator (Misonix, Farmingdale, NY, USA) until it became a milky white color, after which the microPET was allowed to settle to the bottom of the bottle overnight. The upper aqueous layer was carefully decanted to separate the nanoPET suspension from the microPET present in the bottom layer.

#### 4.7.2. BHET and PET Hydrolysis Assay

Degradation of BHET by EstB was assayed as previously described [86]. BHET buffer was made by adding BHET (Sigma-Aldrich, St. Louis, MO, USA) to 1 mM in 40 mM NaH<sub>2</sub>PO<sub>4</sub>, 80 mM NaCl, 20% (v/v) DMSO, pH 7.5 and stirred overnight to dissolve. Complete dissolution of the BHET particles was not observed, but their size was dramatically reduced to an estimated microparticle size (<300 μm). EstB (50 μg) was added to 1 mL of BHET buffer and incubated shaking at 40 °C overnight. Blank assays, in which no protein was added, were used as controls. All assays were performed in triplicate.

The concentration of SDS in the microPET suspension was dramatically reduced by centrifuging the microPET suspension at 12,000 rpm and removing the supernatant before adding an equal volume of Ultrapure water. This procedure was repeated three times to yield a microPET suspension with a very low SDS concentration. EstB (100 μg) was added to 1 mL of PET buffer (40 mM Tris-HCl, 0.8 mM CaCl<sub>2</sub>, 1 mL washed microPET, 20% (v/v) DMSO, pH 8) and incubated shaking at 40 °C overnight. Blank assays, in which no protein was added, were used as controls. All assays were performed in triplicate.

#### 4.7.3. PET Monomer Analysis Using HPLC

Analysis of PET oligomers and monomers were adapted from Furukawa et al. 2019 [87] using an Agilent Technologies 1100 series HPLC equipped with a ZORBAX Eclipse Plus C18 (Rapid Resolution, 4.6 × 100 mm 3.5 Micron) column (Agilent Technologies, Santa Clara, CA, USA). The flow rate, mobile phase, and oven temperature were as previously described [87]. Hydrolyzed products were observed at 254 nM, with a reference at 354 nM. TPA and BHET standards were used to detect peak retention times. The column used in this experiment resulted in significantly shorter retention times compared to previous literature values. Retention times on average for TPA at 1.5 min and BHET at 1.9 min. Experimentally, MHET was expected around 1.7 min.

## 5. Conclusions

Plastic pollution is choking our planet, with more of these materials being made and released into marine and terrestrial environments every year. Though occurring at a slow pace, microbes are able to degrade these man-made polymers. Species of bacteria, including *Pseudomonas* and *Bacillus*, have been implicated in the biodegradation of PET plastic, but very few specific enzymes within these organisms have been identified and characterized [88] (ref). Here we use “omics” approaches and existing databases to elucidate the genetic basis of how a consortium of soil bacteria can cooperate to degrade PET plastic, a model for how this may be occurring in the environment. Using molecular techniques, we identified a new EstB PETase encoded in *Pseudomonas* spp., an initial

depolymerizer, with the potential for additional PETases to be identified and characterized within the pangenome. Unlike bacteria isolated from plastic in marine environments, these *Pseudomonas* and *Bacillus* bacteria isolated from petroleum polluted soils have robust plastic- and plasticizer-degrading capabilities, including 250 associated enzymes among five strains, demonstrating the potential for biodegradation of mixed plastic waste.

**Supplementary Materials:** The following supporting information can be downloaded at: <https://www.mdpi.com/article/10.3390/ijms23105612/s1>.

**Author Contributions:** Conceptualization, S.E., J.L.M. and R.L.-Z.; methodology, S.E., J.L.M. and R.L.-Z.; software, R.L.-Z.; validation, S.E., R.D., H.L. and T.B.; formal analysis, S.E., G.S., O.A. and R.L.-Z.; investigation, S.E., R.D., H.L.; resources, J.L.M. and R.L.-Z.; data curation, S.E. and R.L.-Z.; writing—original draft preparation, S.E.; writing—review and editing, S.E., R.D., H.L., G.S., O.A., T.B., R.L.-Z. and J.L.M.; visualization, S.E., R.D., H.L.; supervision, J.L.M.; project administration, S.E. and J.L.M.; funding acquisition, J.L.M. All authors have read and agreed to the published version of the manuscript.

**Funding:** This research was funded by NSF RUI Collaborative grant number 1931150, awarded to J.L.M. and R.L.-Z., and in part, by Reed Biology Undergraduate Research Project grants awarded to R.D. and T.B.

**Data Availability Statement:** RNAseq datasets were deposited in the NCBI's Sequence Read Archive (SRA) and are publicly available on GenBank, BioProject Accession PRJNA517285.

**Acknowledgments:** We acknowledge Keith Karoly, Reed Professor of Biology, for his purchase and donation of Biology EcoPlates®.

**Conflicts of Interest:** The authors declare no conflict of interest. The funders had no role in the design of the study; in the collection, analyses, or interpretation of data; in the writing of the manuscript, or in the decision to publish the results.

## References

1. Geyer, R.; Jambeck, J.R.; Law, K.L. Production, Use, and Fate of All Plastics Ever Made. *Sci. Adv.* **2017**, *3*, e1700782. [CrossRef]
2. Plastic Oceans International. Available online: <https://plasticoceans.org/the-facts/> (accessed on 27 April 2022).
3. Peng, Y.; Wu, P.; Schartup, A.T.; Zhang, Y. Plastic Waste Release Caused by COVID-19 and Its Fate in the Global Ocean. *Proc. Natl. Acad. Sci. USA* **2021**, *118*, e2111530118. [CrossRef]
4. Shams, M.; Alam, I.; Mahbub, M.S. Plastic Pollution during COVID-19: Plastic Waste Directives and Its Long-Term Impact on the Environment. *Environ. Adv.* **2021**, *5*, 100119. [CrossRef]
5. Jambeck, J.R.; Geyer, R.; Wilcox, C.; Siegler, T.R.; Perryman, M.; Andrady, A.; Narayan, R.; Law, K.L. Plastic Waste Inputs from Land into the Ocean. *Science* **2015**, *347*, 768–771. [CrossRef]
6. Galloway, T.S. Micro- and Nano-Plastics and Human Health. In *Marine Anthropogenic Litter*; Bergmann, M., Gutow, L., Klages, M., Eds.; Springer International Publishing: Cham, Switzerland, 2015; pp. 343–366. [CrossRef]
7. Jâms, I.B.; Windsor, F.M.; Poudevigne-Durance, T.; Ormerod, S.J.; Durance, I. Estimating the Size Distribution of Plastics Ingested by Animals. *Nat. Commun.* **2020**, *11*, 1594. [CrossRef]
8. Chae, Y.; An, Y.-J. Current Research Trends on Plastic Pollution and Ecological Impacts on the Soil Ecosystem: A Review. *Environ. Pollut.* **2018**, *240*, 387–395. [CrossRef]
9. Gross, L.; Enck, J. Confronting Plastic Pollution to Protect Environmental and Public Health. *PLoS Biol.* **2021**, *19*, e3001131. [CrossRef]
10. Christman, G.D.; León-Zayas, R.I.; Zhao, R.; Summers, Z.M.; Biddle, J.F. Novel Clostridial Lineages Recovered from Metagenomes of a Hot Oil Reservoir. *Sci. Rep.* **2020**, *10*, 8048. [CrossRef]
11. Brahney, J.; Hallerud, M.; Heim, E.; Hahnenberger, M.; Sukumaran, S. Plastic Rain in Protected Areas of the United States. *Science* **2020**, *368*, 1257–1260. [CrossRef]
12. Danso, D.; Chow, J.; Streit, W.R. Plastics: Environmental and Biotechnological Perspectives on Microbial Degradation. *Appl. Environ. Microbiol.* **2019**, *19*, e01095-19. [CrossRef]
13. Kale, S.; Deshmukh, A.G.; Dudhare, M.; Patil, V. Microbial Degradation Of Plastic—A Review. *J. Biochem. Technol.* **2015**, *6*, 952–961. [CrossRef]
14. Mohanan, N.; Montazer, Z.; Sharma, P.K.; Levin, D.B. Microbial and Enzymatic Degradation of Synthetic Plastics. *Front. Microbiol.* **2020**, *11*, 580709. [CrossRef]
15. Zrimec, J.; Kokina, M.; Jonasson, S.; Zorrilla, F.; Zelezniak, A. Plastic-Degrading Potential across the Global Microbiome Correlates with Recent Pollution Trends. *MBio* **2021**, *12*, e02155-21. [CrossRef]

16. Yoshida, S.; Hiraga, K.; Takehana, T.; Taniguchi, I.; Yamaji, H.; Maeda, Y.; Toyohara, K.; Miyamoto, K.; Kimura, Y.; Oda, K. A Bacterium That Degrades and Assimilates Poly(Ethylene Terephthalate). *Science* **2016**, *351*, 1196–1199. [[CrossRef](#)]
17. Tanasupawat, S.; Takehana, T.; Yoshida, S.; Hiraga, K.; Oda, K. *Ideonella Sakaiensis* sp. Nov., Isolated from a Microbial Consortium That Degrades Poly(Ethylene Terephthalate). *Int. J. Syst. Evol. Microbiol.* **2016**, *66*, 2813–2818. [[CrossRef](#)]
18. Sulaiman, S.; Yamato, S.; Kanaya, E.; Kim, J.J.; Koga, Y.; Takano, K.; Kanaya, S. Isolation of a Novel Cutinase Homolog with Polyethylene Terephthalate-Degrading Activity from Leaf-Branch Compost by Using a Metagenomic Approach. *Appl. Environ. Microbiol.* **2012**, *78*, 1556–1562. [[CrossRef](#)]
19. Zhang, T.; Zhang, H. Microbial Consortia Are Needed to Degrade Soil Pollutants. *Microorganisms* **2022**, *10*, 261. [[CrossRef](#)]
20. Bharti, V.; Gupta, B.; Kaur, J. Novel Bacterial Strains *Pseudomonas* sp. and *Bacillus* sp. Isolated from Petroleum Oil Contaminated Soils for Degradation of Flourene and Phenanthrene. *Pollution* **2019**, *5*, 657–669. [[CrossRef](#)]
21. Carniel, A.; Valoni, É.; Nicomedes, J.; da Conceição Gomes, A.; de Castro, A.M. Lipase from *Candida Antarctica* (CALB) and Cutinase from *Humicola Insolens* Act Synergistically for PET Hydrolysis to Terephthalic Acid. *Process Biochem.* **2017**, *59*, 84–90. [[CrossRef](#)]
22. Meyer-Cifuentes, I.E.; Werner, J.; Jehmlich, N.; Will, S.E.; Neumann-Schaal, M.; Öztürk, B. Synergistic Biodegradation of Aromatic-Aliphatic Copolyester Plastic by a Marine Microbial Consortium. *Nat. Commun.* **2020**, *11*, 5790. [[CrossRef](#)]
23. Huerta Lwanga, E.; Thapa, B.; Yang, X.; Gertsen, H.; Salánki, T.; Geissen, V.; Garbeva, P. Decay of Low-Density Polyethylene by Bacteria Extracted from Earthworm's Guts: A Potential for Soil Restoration. *Sci. Total Environ.* **2018**, *624*, 753–757. [[CrossRef](#)]
24. Shah, Z.; Gulzar, M.; Hasan, F.; Shah, A.A. Degradation of Polyester Polyurethane by an Indigenously Developed Consortium of *Pseudomonas* and *Bacillus* Species Isolated from Soil. *Polym. Degrad. Stab.* **2016**, *134*, 349–356. [[CrossRef](#)]
25. Roberts, C.; Edwards, S.; Vague, M.; León-Zayas, R.; Scheffer, H.; Chan, G.; Swartz, N.A.; Mellies, J.L. Environmental Consortium Containing *Pseudomonas* and *Bacillus* Species Synergistically Degrades Polyethylene Terephthalate Plastic. *mSphere* **2020**, *6*, e01151-20. [[CrossRef](#)]
26. Das, N.; Chandran, P. Microbial Degradation of Petroleum Hydrocarbon Contaminants: An Overview. *Biotechnol. Res. Int.* **2010**, *2011*, e941810. [[CrossRef](#)]
27. Leon-Zayas, R.; Roberts, C.; Vague, M.; Mellies, J.L. Draft Genome Sequences of Five Environmental Bacterial Isolates That Degrade Polyethylene Terephthalate Plastic. *Microbiol. Resour. Announc.* **2019**, *8*, e00237-19. [[CrossRef](#)]
28. Medini, D.; Donati, C.; Tettelin, H.; Massignani, V.; Rappuoli, R. The Microbial Pan-Genome. *Curr. Opin. Genet. Dev.* **2005**, *15*, 589–594. [[CrossRef](#)]
29. Pacheco-Moreno, A.; Stefanato, F.L.; Ford, J.J.; Trippel, C.; Uszkoreit, S.; Ferrafiat, L.; Grenga, L.; Dickens, R.; Kelly, N.; Kingdon, A.D.; et al. Pan-Genome Analysis Identifies Intersecting Roles for *Pseudomonas* Specialized Metabolites in Potato Pathogen Inhibition. *eLife* **2021**, *10*, e71900. [[CrossRef](#)]
30. Blaustein, R.A.; McFarland, A.G.; Ben Maamar, S.; Lopez, A.; Castro-Wallace, S.; Hartmann, E.M. Pangenomic Approach To Understanding Microbial Adaptations within a Model Built Environment, the International Space Station, Relative to Human Hosts and Soil. *mSystems* **2019**, *4*, e00281-18. [[CrossRef](#)]
31. Polz, M.F.; Alm, E.J.; Hanage, W.P. Horizontal Gene Transfer and the Evolution of Bacterial and Archaeal Population Structure. *Trends Genet.* **2013**, *29*, 170–175. [[CrossRef](#)]
32. Gonzales-Siles, L.; Karlsson, R.; Schmidt, P.; Salvà-Serra, F.; Jaén-Luchoro, D.; Skovbjerg, S.; Moore, E.R.B.; Gomila, M. A Pangenome Approach for Discerning Species-Unique Gene Markers for Identifications of *Streptococcus Pneumoniae* and *Streptococcus Pseudopneumoniae*. *Front. Cell. Infect. Microbiol.* **2020**, *10*, 222. [[CrossRef](#)]
33. Hara, H.; Eltis, L.D.; Davies, J.E.; Mohn, W.W. Transcriptomic Analysis Reveals a Bifurcated Terephthalate Degradation Pathway in *Rhodococcus* sp. Strain RHA1. *J. Bacteriol.* **2007**, *189*, 1641–1647. [[CrossRef](#)]
34. Croucher, N.J.; Thomson, N.R. Studying Bacterial Transcriptomes Using RNA-Seq. *Curr. Opin. Microbiol.* **2010**, *13*, 619–624. [[CrossRef](#)]
35. Kumari, A.; Bano, N.; Bag, S.K.; Chaudhary, D.R.; Jha, B. Transcriptome-Guided Insights Into Plastic Degradation by the Marine Bacterium. *Front. Microbiol.* **2021**, *12*, 751571. [[CrossRef](#)]
36. Gan, Z.; Zhang, H. PMBD: A Comprehensive Plastics Microbial Biodegradation Database. *Database* **2019**, *2019*, baz119. [[CrossRef](#)]
37. Vallenet, D.; Calteau, A.; Dubois, M.; Amours, P.; Bazin, A.; Beuvin, M.; Burlot, L.; Bussell, X.; Fouteau, S.; Gautreau, G.; et al. MicroScope: An Integrated Platform for the Annotation and Exploration of Microbial Gene Functions through Genomic, Pangenomic and Metabolic Comparative Analysis. *Nucleic Acids Res.* **2020**, *48*, D579–D589. [[CrossRef](#)]
38. Miele, V.; Penel, S.; Duret, L. Ultra-Fast Sequence Clustering from Similarity Networks with SiLiX. *BMC Bioinform.* **2011**, *12*, 116. [[CrossRef](#)]
39. Qiu, L.; Yin, X.; Liu, T.; Zhang, H.; Chen, G.; Wu, S. Biodegradation of Bis(2-Hydroxyethyl) Terephthalate by a Newly Isolated *Enterobacter* sp. *HY1* and Characterization of Its Esterase Properties. *J. Basic Microbiol.* **2020**, *60*, 699–711. [[CrossRef](#)]
40. Huang, W.; Wilks, A. A Rapid Seamless Method for Gene Knockout in *Pseudomonas Aeruginosa*. *BMC Microbiol.* **2017**, *17*, 199. [[CrossRef](#)]
41. Jumper, J.; Evans, R.; Pritzel, A.; Green, T.; Figurnov, M.; Ronneberger, O.; Tunyasuvunakool, K.; Bates, R.; Žídek, A.; Potapenko, A.; et al. Highly Accurate Protein Structure Prediction with AlphaFold. *Nature* **2021**, *596*, 583–589. [[CrossRef](#)]
42. Joo, S.; Cho, I.J.; Seo, H.; Son, H.F.; Sagong, H.-Y.; Shin, T.J.; Choi, S.Y.; Lee, S.Y.; Kim, K.-J. Structural Insight into Molecular Mechanism of Poly(Ethylene Terephthalate) Degradation. *Nat. Commun.* **2018**, *9*, 382. [[CrossRef](#)]

43. Austin, H.P.; Allen, M.D.; Donohoe, B.S.; Rorrer, N.A.; Kearns, F.L.; Silveira, R.L.; Pollard, B.C.; Dominick, G.; Duman, R.; El Omari, K.; et al. Characterization and Engineering of a Plastic-Degrading Aromatic Polyesterase. *Proc. Natl. Acad. Sci. USA* **2018**, *115*, E4350–E4357. [[CrossRef](#)]
44. Herold, D.A.; Keil, K.; Bruns, D.E. Oxidation of Polyethylene Glycols by Alcohol Dehydrogenase. *Biochem. Pharmacol.* **1989**, *38*, 73–76. [[CrossRef](#)]
45. Rogers, J.D.; Thurman, E.M.; Ferrer, I.; Rosenblum, J.S.; Evans, M.V.; Mouser, P.J.; Ryan, J.N. Degradation of Polyethylene Glycols and Polypropylene Glycols in Microcosms Simulating a Spill of Produced Water in Shallow Groundwater. *Environ. Sci. Process. Impacts* **2019**, *21*, 256–268. [[CrossRef](#)]
46. Sunny; Maurya, A.; Vats, M.K.; Khare, S.K.; Srivastava, K.R. Computational Exploration of Bio-Remediation Solution for Mixed Plastic Waste. *BioRxiv* **2022**, 485065. [[CrossRef](#)]
47. Hou, L.; Majumder, E.L.-W. Potential for and Distribution of Enzymatic Biodegradation of Polystyrene by Environmental Microorganisms. *Materials* **2021**, *14*, 503. [[CrossRef](#)]
48. Gambarini, V.; Pantos, O.; Kingsbury, J.M.; Weaver, L.; Handley, K.M.; Lear, G. Phylogenetic Distribution of Plastic-Degrading Microorganisms. *MSystems* **2021**, *6*, e01112–20. [[CrossRef](#)]
49. Rabodonirina, S.; Rasolomampianina, R.; Krier, F.; Drider, D.; Merhaby, D.; Net, S.; Ouddane, B. Degradation of Fluorene and Phenanthrene in PAHs-Contaminated Soil Using *Pseudomonas* and *Bacillus* Strains Isolated from Oil Spill Sites. *J. Environ. Manage.* **2019**, *232*, 1–7. [[CrossRef](#)]
50. Ghosal, D.; Ghosh, S.; Dutta, T.K.; Ahn, Y. Current State of Knowledge in Microbial Degradation of Polycyclic Aromatic Hydrocarbons (PAHs): A Review. *Front. Microbiol.* **2016**, *7*, 1369. [[CrossRef](#)]
51. Yan, S.; Wu, G. Reorganization of Gene Network for Degradation of Polycyclic Aromatic Hydrocarbons (PAHs) in *Pseudomonas Aeruginosa* PAO1 under Several Conditions. *J. Appl. Genet.* **2017**, *58*, 545–563. [[CrossRef](#)]
52. Boll, M.; Geiger, R.; Junghare, M.; Schink, B. Microbial Degradation of Phthalates: Biochemistry and Environmental Implications. *Environ. Microbiol. Rep.* **2020**, *12*, 3–15. [[CrossRef](#)]
53. Valkova, N.; Lépine, F.; Valeanu, L.; Dupont, M.; Labrie, L.; Bisaillon, J.-G.; Beudet, R.; Shareck, F.; Villemur, R. Hydrolysis of 4-Hydroxybenzoic Acid Esters (Parabens) and Their Aerobic Transformation into Phenol by the Resistant Enterobacter Cloacae Strain EM. *Appl. Environ. Microbiol.* **2001**, *67*, 2404–2409. [[CrossRef](#)]
54. Nichols, N.N.; Harwood, C.S. PcaK, a High-Affinity Permease for the Aromatic Compounds 4-Hydroxybenzoate and Protocatechuate from *Pseudomonas Putida*. *J. Bacteriol.* **1997**, *179*, 5056–5061. [[CrossRef](#)]
55. Harwood, C.S.; Nichols, N.N.; Kim, M.K.; Ditty, J.L.; Parales, R.E. Identification of the PcaRKF Gene Cluster from *Pseudomonas Putida*: Involvement in Chemotaxis, Biodegradation, and Transport of 4-Hydroxybenzoate. *J. Bacteriol.* **1994**, *176*, 6479–6488. [[CrossRef](#)]
56. Ndahebwa Muhonja, C.; Magoma, G.; Imbuga, M.; Makonde, H.M. Molecular Characterization of Low-Density Polyethylene (LDPE) Degrading Bacteria and Fungi from Dandora Dumpsite, Nairobi, Kenya. *Int. J. Microbiol.* **2018**, *2018*, 4167845. [[CrossRef](#)]
57. Song, C.; Mazzola, M.; Cheng, X.; Oetjen, J.; Alexandrov, T.; Dorrestein, P.; Watrous, J.; van der Voort, M.; Raaijmakers, J.M. Molecular and Chemical Dialogues in Bacteria-Protozoa Interactions. *Sci. Rep.* **2015**, *5*, 12837. [[CrossRef](#)]
58. Jendrossek, D.; Handrick, R. Microbial Degradation of Polyhydroxyalkanoates. *Annu. Rev. Microbiol.* **2002**, *56*, 403–432. [[CrossRef](#)]
59. Donlan, R.M. Biofilms: Microbial Life on Surfaces. *Emerg. Infect. Dis.* **2002**, *8*, 881–890. [[CrossRef](#)]
60. Chen, C.-C.; Han, X.; Ko, T.-P.; Liu, W.; Guo, R.-T. Structural Studies Reveal the Molecular Mechanism of PETase. *FEBS J.* **2018**, *285*, 3717–3723. [[CrossRef](#)]
61. Gu, J.-D. Microbial Colonization of Polymeric Materials for Space Applications and Mechanisms of Biodeterioration: A Review. *Int. Biodeterior. Biodegrad.* **2007**, *59*, 170–179. [[CrossRef](#)]
62. Kyaw, B.M.; Champakalakshmi, R.; Sakharkar, M.K.; Lim, C.S.; Sakharkar, K.R. Biodegradation of Low Density Polythene (LDPE) by *Pseudomonas* Species. *Indian J. Microbiol.* **2012**, *52*, 411–419. [[CrossRef](#)]
63. Das, M.P.; Kumar, S. An Approach to Low-Density Polyethylene Biodegradation by *Bacillus Amylolyquefaciens*. *3 Biotech.* **2015**, *5*, 81–86. [[CrossRef](#)] [[PubMed](#)]
64. Bubpachat, T.; Sombatsompop, N.; Prapagdee, B. Isolation and Role of Polylactic Acid-Degrading Bacteria on Degrading Enzymes Productions and PLA Biodegradability at Mesophilic Conditions. *Polym. Degrad. Stab.* **2018**, *152*, 75–85. [[CrossRef](#)]
65. Bonifer, K.S.; Wen, X.; Hasim, S.; Phillips, E.K.; Dunlap, R.N.; Gann, E.R.; DeBruyn, J.M.; Reynolds, T.B. *Bacillus Pumilus* B12 Degrades Polylactic Acid and Degradation Is Affected by Changing Nutrient Conditions. *Front. Microbiol.* **2019**, *10*, 2548. [[CrossRef](#)] [[PubMed](#)]
66. Suzuki, T.; Ichihara, Y.; Yamada, M.; Tonomura, K. Some Characteristics of *Pseudomonas* 0–3 Which Utilizes Polyvinyl Alcohol. *Agric. Biol. Chem.* **1973**, *37*, 747–756. [[CrossRef](#)]
67. Rolsky, C.; Kelkar, V. Degradation of Polyvinyl Alcohol in US Wastewater Treatment Plants and Subsequent Nationwide Emission Estimate. *Int. J. Environ. Res. Public Health* **2021**, *18*, 6027. [[CrossRef](#)] [[PubMed](#)]
68. Hahladakis, J.N.; Velis, C.A.; Weber, R.; Iacovidou, E.; Purnell, P. An Overview of Chemical Additives Present in Plastics: Migration, Release, Fate and Environmental Impact during Their Use, Disposal and Recycling. *J. Hazard. Mater.* **2018**, *344*, 179–199. [[CrossRef](#)]
69. Keresztes, S.; Tatár, E.; Czégény, Z.; Záray, G.; Mihucz, V.G. Study on the Leaching of Phthalates from Polyethylene Terephthalate Bottles into Mineral Water. *Sci. Total Environ.* **2013**, *458–460*, 451–458. [[CrossRef](#)]

70. Abboudi, M.; Odeh, A.; Aljoumaa, K. Carbonyl Compound Leaching from Polyethylene Terephthalate into Bottled Water under Sunlight Exposure. *Toxicol. Environ. Chem.* **2016**, *98*, 167–178. [CrossRef]
71. Darbre, P.D.; Harvey, P.W. Paraben Esters: Review of Recent Studies of Endocrine Toxicity, Absorption, Esterase and Human Exposure, and Discussion of Potential Human Health Risks. *J. Appl. Toxicol.* **2008**, *28*, 561–578. [CrossRef]
72. Dutta, S.; Haggerty, D.K.; Rappolee, D.A.; Ruden, D.M. Phthalate Exposure and Long-Term Epigenomic Consequences: A Review. *Front. Genet.* **2020**, *11*, 405. [CrossRef]
73. Baloyi, N.D.; Tekere, M.; Maphangwa, K.W.; Masindi, V. Insights Into the Prevalence and Impacts of Phthalate Esters in Aquatic Ecosystems. *Front. Environ. Sci.* **2021**, *9*, 684190. [CrossRef]
74. Wagner, S.; Schlummer, M. Legacy Additives in a Circular Economy of Plastics: Current Dilemma, Policy Analysis, and Emerging Countermeasures. *Resour. Conserv. Recycl.* **2020**, *158*, 104800. [CrossRef]
75. Plass, C.; Hiessl, R.; Kleber, J.; Grimm, A.; Langsch, A.; Otter, R.; Liese, A.; Gröger, H. Towards Bio-Based Plasticizers with Reduced Toxicity: Synthesis and Performance Testing of a 3-Methylphthalate. *Sustain. Chem. Pharm.* **2020**, *18*, 100319. [CrossRef]
76. Jamarani, R.; Erythropel, H.C.; Nicell, J.A.; Leask, R.L.; Marić, M. How Green Is Your Plasticizer? *Polymers* **2018**, *10*, 834. [CrossRef] [PubMed]
77. Stark, L.; Giersch, T.; Wünschiers, R. Efficiency of RNA Extraction from Selected Bacteria in the Context of Biogas Production and Metatranscriptomics. *Anaerobe* **2014**, *29*, 85–90. [CrossRef]
78. Andrews, S. FastQC: A Quality Control Tool for High Throughput Sequence Data. 2010. Available online: <https://www.bioinformatics.babraham.ac.uk/projects/fastqc/> (accessed on 11 February 2022).
79. Chen, S.; Huang, T.; Zhou, Y.; Han, Y.; Xu, M.; Gu, J. AfterQC: Automatic Filtering, Trimming, Error Removing and Quality Control for Fastq Data. *BMC Bioinform.* **2017**, *18*, 80. [CrossRef]
80. Langmead, B.; Salzberg, S.L. Fast Gapped-Read Alignment with Bowtie 2. *Nat. Methods* **2012**, *9*, 357–U54. [CrossRef]
81. Li, H.; Handsaker, B.; Wysoker, A.; Fennell, T.; Ruan, J.; Homer, N.; Marth, G.; Abecasis, G.; Durbin, R.; 1000 Genome Project Data Processing Subgroup. The Sequence Alignment/Map Format and SAMtools. *Bioinformatics* **2009**, *25*, 2078–2079. [CrossRef]
82. Liao, Y.; Smyth, G.K.; Shi, W. FeatureCounts: An Efficient General Purpose Program for Assigning Sequence Reads to Genomic Features. *Bioinformatics* **2014**, *30*, 923–930. [CrossRef]
83. Love, M.I.; Huber, W.; Anders, S. Moderated Estimation of Fold Change and Dispersion for RNA-Seq Data with DESeq2. *Genome Biol.* **2014**, *15*, 550. [CrossRef]
84. Robinson, M.D.; McCarthy, D.J.; Smyth, G.K. EdgeR: A Bioconductor Package for Differential Expression Analysis of Digital Gene Expression Data. *Bioinformatics* **2010**, *26*, 139–140. [CrossRef] [PubMed]
85. Rodríguez-Hernández, A.G.; Muñoz-Tabares, J.A.; Aguilar-Guzmán, J.C.; Vazquez-Duhalt, R. A Novel and Simple Method for Polyethylene Terephthalate (PET) Nanoparticle Production. *Environ. Sci. Nano* **2019**, *6*, 2031–2036. [CrossRef]
86. Palm, G.J.; Reisky, L.; Böttcher, D.; Müller, H.; Michels, E.A.P.; Walczak, M.C.; Berndt, L.; Weiss, M.S.; Bornscheuer, U.T.; Weber, G. Structure of the Plastic-Degrading *Ideonella Sakaiensis* MHETase Bound to a Substrate. *Nat. Commun.* **2019**, *10*, 1717. [CrossRef] [PubMed]
87. Furukawa, M.; Kawakami, N.; Tomizawa, A.; Miyamoto, K. Efficient Degradation of Poly(Ethylene Terephthalate) with *Thermobifida Fusca* Cutinase Exhibiting Improved Catalytic Activity Generated Using Mutagenesis and Additive-Based Approaches. *Sci. Rep.* **2019**, *9*, 16038. [CrossRef]
88. Magalhães, R.P.; Cunha, J.M.; Sousa, S.F. Perspectives on the Role of Enzymatic Biocatalysis for the Degradation of Plastic PET. *Int. J. Mol. Sci.* **2021**, *22*, 11257. [CrossRef]